remote sensing

MDPI

Article

Long-Term Land Use/Land Cover Change Assessment of the Kilombero Catchment in Tanzania Using Random Forest Classification and Robust Change Vector Analysis

Frank Thonfeld [1,2,*], Stefanie Steinbach [3], Javier Muro [4] and Fridah Kirimi [5]

1 German Remote Sensing Data Center (DFD), German Aerospace Center (DLR), Münchener Straße 20, 82234 Weßling, Germany
2 Department of Remote Sensing, University of Würzburg, Oswald-Külpe-Str. 86, 97074 Würzburg, Germany
3 Faculty of Geo-Information Science and Earth Observation (ITC), University of Twente, Hengelosestraat 99, 7514 AE Enschede, The Netherlands; s.steinbach@utwente.nl
4 Center for Remote Sensing of Land Surfaces (ZFL), University of Bonn, 53113 Bonn, Germany; jmuro@uni-bonn.de
5 Department of Geomatic Engineering and Geospatial Information Systems, Jomo Kenyatta University of Agriculture and Technology, P.O. Box 62000 Nairobi, Kenya; fkirimi@jkuat.ac.ke
* Correspondence: frank.thonfeld@dlr.de; Tel.: +49-8153-28-4306

Received: 29 January 2020; Accepted: 21 March 2020; Published: 25 March 2020

Abstract: Information about land use/land cover (LULC) and their changes is useful for different stakeholders to assess future pathways of sustainable land use for food production as well as for nature conservation. In this study, we assess LULC changes in the Kilombero catchment in Tanzania, an important area of recent development in East Africa. LULC change is assessed in two ways: first, post-classification comparison (PCC) which allows us to directly assess changes from one LULC class to another, and second, spectral change detection. We perform LULC classification by applying random forests (RF) on sets of multitemporal metrics that account for seasonal within-class dynamics. For the spectral change detection, we make use of the robust change vector analysis (RCVA) and determine those changes that do not necessarily lead to another class. The combination of the two approaches enables us to distinguish areas that show (a) only PCC changes, (b) only spectral changes that do not affect the classification of a pixel, (c) both types of change, or (d) no changes at all. Our results reveal that only one-quarter of the catchment has not experienced any change. One-third shows both, spectral changes and LULC conversion. Changes detected with both methods predominantly occur in two major regions, one in the West of the catchment, one in the Kilombero floodplain. Both regions are important areas of food production and economic development in Tanzania. The Kilombero floodplain is a Ramsar protected area, half of which was converted to agricultural land in the past decades. Therefore, LULC monitoring is required to support sustainable land management. Relatively poor classification performances revealed several challenges during the classification process. The combined approach of PCC and RCVA allows us to detect spatial patterns of LULC change at distinct dimensions and intensities. With the assessment of additional classifier output, namely class-specific per-pixel classification probabilities and derived parameters, we account for classification uncertainty across space. We overlay the LULC change results and the spatial assessment of classification reliability to provide a thorough picture of the LULC changes taking place in the Kilombero catchment.

Keywords: land-use/land-cover change; robust change vector analysis; Kilombero; wetland; food production; random forest; multitemporal metrics; Landsat; post-classification comparison

1. Introduction

Land use and land cover (LULC) and their change are key drivers of global change [1]. Over the past two decades, land-use change has accelerated, particularly in sub-Saharan Africa. The main reasons for this are growing population and consequently increasing demand for food and space. LULC change puts ecosystems under pressure. Hence, wetlands—traditionally untouched landscapes—were discovered as potential food production zones due to their capacities to reliably provide clean water and therefore good conditions for agricultural production and numerous other ecosystem services [2]. Natural wetlands, however, are among the most threatened ecosystems with a decline in area of approx. 35% between 1970 and 2015 [3–5]. Within the multi-disciplinary research project "GlobE—Wetlands in East Africa", challenges of stagnating or declining trends in food production and nature protection were addressed for four representative wetland sites in Kenya, Rwanda, Uganda and Tanzania. The objectives of the project were the assessment of wetland contribution to food security and of the sustainability of current wetland uses, as well as the spatio-temporal extrapolation of results through simulation modeling and scenarios. Knowledge of land cover holds quantified and spatially explicit information as an imprint of socio-economic activity in wetland landscapes and can be integrated in hydrological and agricultural modeling [6]. However, such data is particularly scarce in many African regions. Earth Observation provides the means for detailed inventory, status and trend analysis, and long-term monitoring [7,8]. The present study therefore focuses on the remote sensing based long-term LULC change assessment in the Tanzanian Kilombero catchment.

Knowledge of the land surface is crucial, since primary production takes place at the land surface, making it the key resource for all animals and human beings. In turn, LULC become central ecosystem indicators [9]. However, extensive and repeated information on LULC for the Kilombero catchment is limited. First scientific assessments of the Kilombero valley ecosystem characterizing geology as well as LULC and economic specifications emerged in the 1960s [10,11]. Attention was put on the Kilombero area again since it became increasingly important for Tanzania's agricultural production. Recent publications focus on hydrological impacts of LULC change within the Kilombero catchment [6,12,13]. They reveal a high dependency of the wetland on baseflow contribution from the enclosing catchment and demonstrate strong impacts of anthropogenic LULC change on water balance components at subcatchment scale.

LULC classification in the context of wetlands is often complicated by frequent, sometimes persistent cloud cover and high air moisture content leading to reduced data availability of optical images compared to other regions. Wetlands are dynamic systems with sometimes substantial intra- and interseasonal variation [14]. Therefore, optimal acquisition times for repeated assessments usually do not exist. To capture specific events such as floods or specific features such as peak season it is most beneficial to take into account all available information. Although various approaches to assess wetlands were published recently [15,16] their analysis is often limited to the actual wetland area and usually a buffer around it. Catchment-wide studies are rare, in particular in East Africa. LULC change in the Kilombero valley was addressed in several case studies [6,12,17–26]. Only a few of these studies explored the whole catchment and only few provided an exhaustive evaluation of the generated LULC change maps. LULC maps are needed, however, to balance the different interests in the catchment, to support local authorities and to implement policies [20].

With this study we want to assess and quantify LULC of the Kilombero catchment, Tanzania, and their changes over the past 45 years. The underlying research questions are to which extent and where LULC changes have occurred and of which nature these changes are. This spatially explicit information is needed to address land management in the Kilombero valley. Our objective is further to address major challenges occurring during the classification and change detection process. Post-classification comparison (PCC) is a common technique to assess LULC changes [27,28]. This well-established technique is prone to error propagation because errors from both the first and the second classification translate into the resulting map. Therefore, change tends to be overestimated. To reduce this source of error, PCC can be combined with spectral change detection methods [29]. Applying a threshold allows

us to differentiate changed from unchanged areas. Assuming that only areas with strong spectral changes translate in a new classification, map update is often applied only to changed areas [30]. A further objective of this study is hence to analyze the correlation of PCC and spectral changes in order to achieve better understanding of the results. In addition, we explore the per-pixel classification probabilities to identify regions of different classifier reliability. Even though many machine learning algorithms provide probabilities as secondary output, these are not considered in most studies. The rest of the paper is organized as follows. In Section 2, we introduce the study site and describe satellite and field data and their processing. This section also includes a description of the LULC mapping and change detection approach and a protocol of the accuracy assessment. Section 3 presents major findings of this study and a thorough discussion; Section 4 briefly presents a conclusion.

2. Materials and Methods

2.1. Study Area

The Kilombero catchment (Figure 1) is located in southern Tanzania and covers an area of 40,240 km^2. It contains a vast floodplain wetland at an elevation of about 200–250 m above sea level. The Udzungwa mountains adjacent to the floodplain in the north and northwest reach an elevation of approx. 2500 m above sea level [31]. The Mahenge mountains further bound the valley zone in the south, and an undulating peneplain borders it to the west [11]. According to the Köppen-Geiger climate classification [32,33], the study area lies in the bioclimatic zone of "tropical savannah" (Aw), and the mean temperature and annual rainfall are 25°C and 1418 mm in Ifakara, the largest town in the catchment. Woodlands and edaphic grasslands compose the natural vegetation [34]. However, due to the large extent of the catchment spanning across various topographic zones, rainfall patterns change with more orographic rainfall towards the Great Escarpment mountains and less rainfall in flatter areas [11]. There are two rainy seasons: a short one between November and January and a long one from March to May. A distinct dry season stretches from July to October [35,36]. The Kilombero river is a naturally shaped tributary of the Rufiji river with a high yearly discharge variability of about 92–3044 m^3/s—as observed at the Swero gauging station situated close to the outlet of the catchment—and regular extensive flooding of the wetland during the long rainy season [20,37,38].

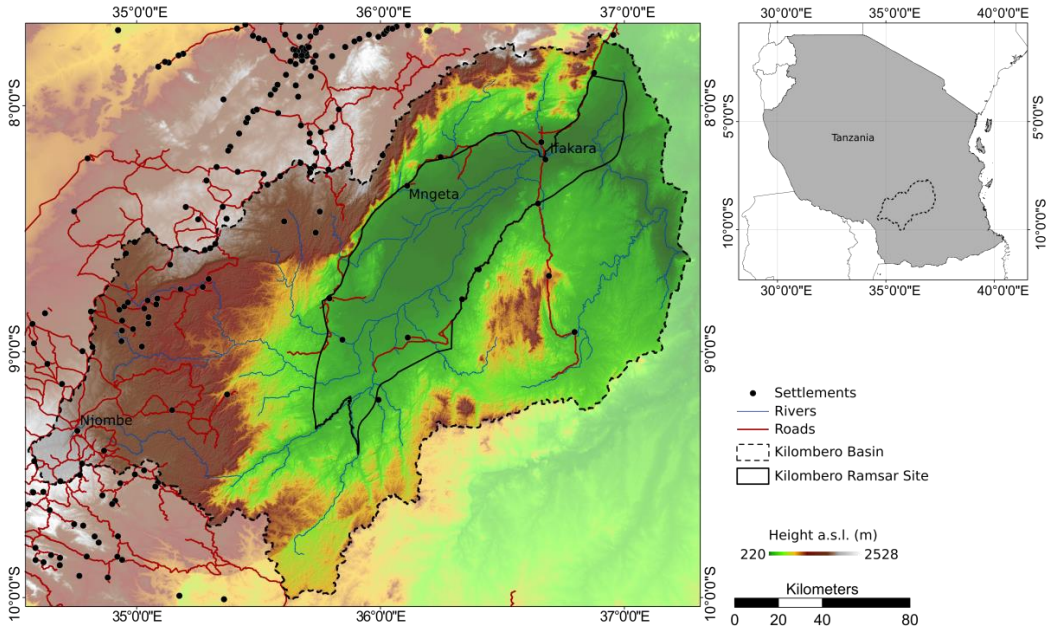

Figure 1. Digital elevation model of the Kilombero catchment overlaid by roads and river networks, settlements, and the Kilombero Ramsar site outline (data source: Open Street Map (OSM): www.openstreetmap.org, United States Geological Survey (USGS): https://earthexplorer.usgs.gov/).

The Kilombero wetland is classified as an important bird area and was included in the Ramsar Convention on Wetlands list of wetlands of international importance in 2002.

The only connection of the Kilombero and Ulanga districts north and south of the Kilombero River was a ferry until 2017, when a bridge was finally installed after several attempts. With the recently established bridge and hence improved accessibility of the southern part of the valley, an increased population growth can be expected in the Ulanga district.

The road network inside the Kilombero valley is very loose, and access in particular to the south is limited although the road network is being developed (Figure 1). Rice cultivation in the Kilombero valley began in the mid of the last century. Today, rice production provides the main economic value of the Kilombero floodplain followed by sugarcane, forest products, fishing and livestock [39]. Over the past decades, pastoralist and agro-pastoralist groups of Maasai, Sukuma, and Barbaig have migrated from other Tanzanian regions into the catchment [40]. Consequently, both agricultural and livestock productivity have experienced considerable growth in the 21st century [40]. In the multi-stakeholder setting, land conflicts are sometimes attributed to these recent immigrants as they are often seen as intruders by local villagers and blamed for environmental degradation and threatening of resources. Large-scale farming and large protected areas are further competitors for land. During the past years, teak (*Tectona grandis*) plantations were installed in the uplands mainly south of the Kilombero river [24]. Additionally, smallholder forest plantations are a quickly developing phenomenon throughout south-western Tanzania [41].

2.2. Satellite Data and Pre-Processing

Landsat is the only operational medium spatial resolution earth observation (EO) system providing data covering the last 45 years. Therefore, this study relies on data from the Landsat system. The challenge of wetland monitoring with optical data is that they are often obscured by clouds due to higher evaporation rates caused by higher water availability compared to drylands. Additionally, the mountain ranges surrounding the Kilombero floodplain act as a cloud trap. In this study, we produced decadal LULC maps for 1974, 1994, 2004, and 2014. Since it was not possible to generate a gapless dataset for the 1980s even when the whole decade was considered and different compositing approaches were tested, we had to skip this period. All images from the three time periods (1994, 2004, 2014) ± 1 year with less than 80% cloud cover were downloaded from the United States Geological Survey (USGS) earth explorer (https://earthexplorer.usgs.gov/). Additional 17 images were downloaded for the 1970s. The satellite imagery as of Landsat 5 possesses the same spatial resolution of 30 m, and although bandwidths differ slightly between sensors, the products are nevertheless compatible [42]. The dataset properties are presented in Table 1. Cloud masking was performed using the function of mask (Fmask) output included in the pixel quality files appended to each dataset [43,44]. For each Landsat image we calculated the normalized difference built-up index (NDBI) [45], the normalized difference vegetation index (NDVI) [46], the normalized difference water index (NDWI) [47], and the Tasseled Cap [48,49] components brightness, greenness, and wetness as defined for Landsat surface reflectance data [50]. Image tiles from one orbit (i.e., with identical acquisition dates) were mosaicked to avoid double occurrence of along-track overlapping areas.

Temporal variability is often a challenge of wetland classification since some classes are changing dynamically their condition [14,51–53], e.g., through flooding, pronounced dry phases, or cropping cycles. Several image compositing approaches were developed in the past years [54–62]. The general idea of those methods is to select on a per-pixel basis the most suitable observations from a predefined selection of images that fulfill different quality criteria and represent spectral reflectance of one particular day of year in the best way. As a result, one gapless and cloud free image composed of most suitable observations from multiple – possibly partly clouded – images is generated. However, both high seasonal class variability and high cloud coverage make conventional mosaicking and compositing approaches inadequate for the study area at the given data availability. Therefore, we made use of multitemporal metrics to generate gapless and cloud free synthetic images from a

selection of images with noise (e.g., clouds, cloud shadows, gaps from Landsat 7 scan line corrector failure) [63–68]. Since extreme values may be caused by artifacts such as missed clouds and cloud shadows, percentiles are usually preferred, although actual extreme values may be missed (Figure 2). We used multitemporal metrics (10th percentile, 25th percentile, mean, 75th percentile, 90th percentile) of the six reflective Landsat bands (blue, green, red, near infra-red, and two short-wave infra-red), NDVI, NDBI, NDWI, Tasseled Cap brightness, greenness, and wetness. NDBI and TC brightness are sensitive to non-vegetated areas and settlements; NDVI and TC greenness are useful for discriminating vegetation properties; and NDWI and TC wetness highlight open water bodies.

Table 1. Overview of the applied datasets (MSS = multispectral scanner, TM = thematic mapper, ETM+ = enhanced thematic mapper plus, OLI = operational land imager, SR = surface reflectance).

Target Year	Spatial Resolution	Sensor	Specifications	No. of Images
1974 ± 5 year	60 m resampled to 30 m	Landsat-1/2 MSS	Pre-Collection Level-1	17
1994 ± 1 year	30 m	Landsat-5 TM	SR Level-2 Science Products	100
2004 ± 1 year	30 m	Landsat-5 TM, Landsat-7 ETM+	SR Level-2 Science Products	209
2014 ± 1 year	30 m	Landsat-7 ETM+, Landsat-8 OLI	SR Level-2 Science Products	462

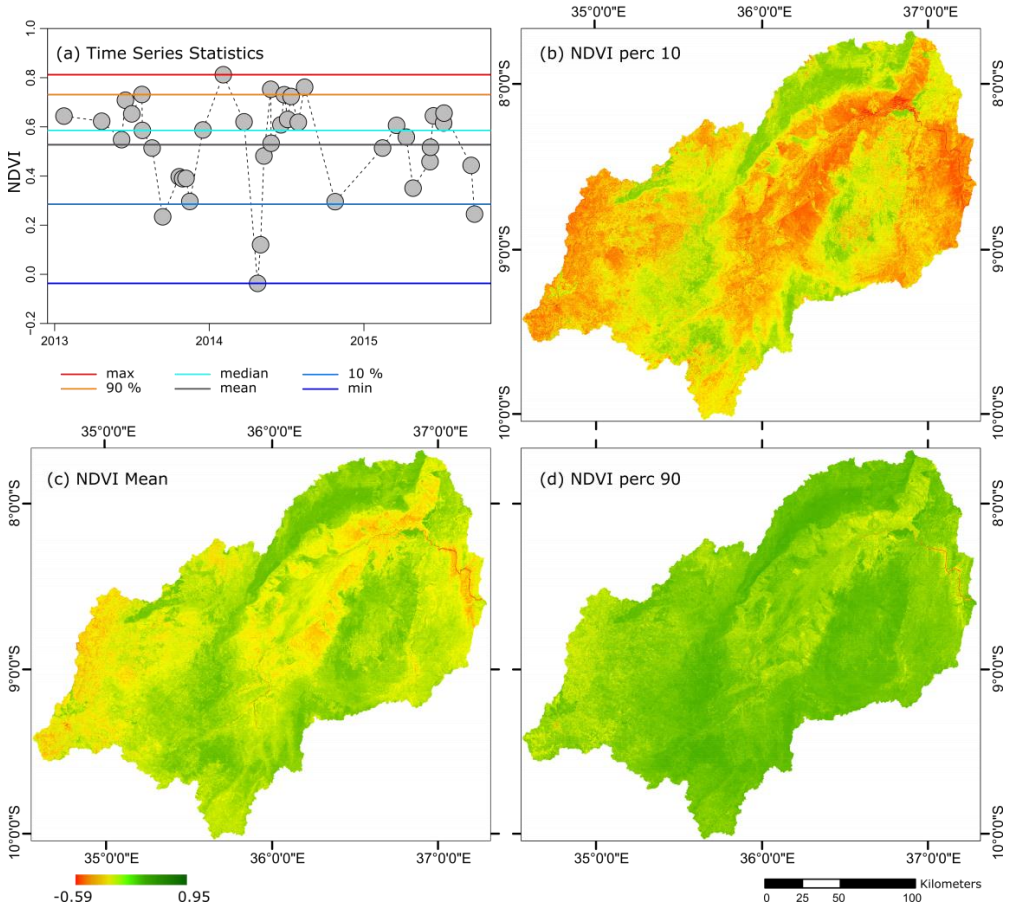

Figure 2. (**a**) Time series of normalized difference vegetation index (NDVI) with colored lines as indicator of minimum, maximum, mean, median, 10th percentile and 90th percentile, (**b**) NDVI 10th percentile, (**c**) NDVI mean, and (**d**) NDVI 90th percentile. Intra-class variability is reflected through the percentiles. However, actual extremes might be missed by percentiles as compared to the extreme values in the time series.

Although the use of NDBI, NDVI, NDWI, and the Tasseled Cap components may appear redundant, the approaches to calculate them are different and make them complementary. Figure 2 exemplary shows the multitemporal minimum, mean and maximum NDVI composites and a schematic presentation of their calculation.

Earlier Landsat products from MSS sensor have a coarser spatial resolution (60 m) and crudely different radiometric characteristics, and were therefore processed in a different way. Individual images were radiometrically normalized to a master image using the iteratively re-weighted multivariate alteration detection (IR-MAD) algorithm [69,70]. Clouds were masked based on manually selected thresholds of image brightness (i.e., the squared root of the sum of all spectral bands) and manual corrections. Finally, the resulting images were mosaicked to one gapless and cloud free image that represents the 1974 period. From that we calculated NDVI and the TC components.

The 30 m resolution shuttle radar topography mission digital elevation model (SRTM DEM) was used to account for the distinct morphology of the Kilombero catchment. The near-global DEM is composed from C-band radar data acquired in 2000 [71]. The data is widely used because of its relatively high and spatially coherent accuracy compared to other global datasets and its availability free of cost [72]. The floodplain wetland developed on the lower part of a fault, whereas the Udzungwa Mountains represent the upper part, leading to harsh differences in elevation and inclination across morphological zones. Since these are associated with land use, land cover, and species composition [73], the main Landsat dataset was complemented with the SRTM DEM and a number of derivatives: the morphometric indices calculated from the SRTM DEM were the terrain ruggedness index (TRI) [74], slope variability (SV) [75], the topographic position index (TPI) [76,77], and for potential soil moisture the topographic wetness index (TWI) [78], which all combine different derivatives of elevation. In addition to those four variables, slope and elevation were used in the classification. TRI, SV, and TPI were calculated using the ArcGIS geomorphometry and gradient toolbox [79].

2.3. Field Data and Other Reference Data

Several field campaigns and uncrewed aerial vehicle (UAV) flight campaigns were conducted between 2013 and 2016 to collect ground information. During three UAV campaigns in 2014 and 2015 a fixed-wing drone took images of ~20 cm spatial resolution in the area around Ifakara (approx. 10×3 km^2). The field campaigns covered dry and rainy season and included trips by foot, motorbike and car, during which global positioning system (GPS) points and photos of regions of interest were taken. We recorded LULC data as well as information about vegetation cover along paths (roads, footpaths, flight paths) for a subset of points. Independently, between 2015 and 2016 the Belgian Development Agency (Enabel, https://www.enabel.be/) conducted flight and road campaigns using a small aircraft and a jeep to collect high resolution imagery of the floodplain. The photos were taken with an action camera tied to the vehicles, and a handheld GPS at 2-second intervals.

Another 28 high-resolution RapidEye scenes were obtained via the RapidEye science archive (RESA) of the German aerospace center (DLR). They were used to complement the ground reference database. The images were captured between 25/08/2013 and 06/06/2015, thus covering almost two years' wet and dry season cycles. The spatial coverage, however, is limited to the northern part of the catchment, including the town of Ifakara. The commercial RapidEye sensors provide a spatial resolution of 6.5 m, 5 spectral bands, and an approximate revisit time of 6.5 days [80]. To complement the ground information, we subdivided the catchment in a regular grid of 25×25 km^2 cells and selected 10 points per grid cell using random sampling. Each point was labeled based on photo interpretation of GoogleEarth and RapidEye images.

2.4. LULC Mapping

To assess long-term LULC changes, we performed a classification based on historical records of remote sensing data. We used a robust classification scheme targeting environmentally and socio-economically important classes, based on an approach that can handle data scarcity and that

can capture variable classes. Our classification scheme includes 11 classes: montane forest, closed woodland, open woodland, teak plantation, swamp, grassland, savanna, upland agriculture, rice, built-up area, and water (Table 2). Open woodland mainly refers to Miombo dry forests (*Brachystegia longifolia*). Upland agriculture comprises maize, vegetables and other food crops usually grown in mosaics of small patches and in crop rotation. In contrast, floodplain agriculture comprises rice fields that rely on the water of the annual Kilombero flooding and its tributaries. Grassland refers to natural flood grassland dominated by sedges such as *Cyperus distans* as described in [11] whereas savanna comprises all non-flooded open grasslands with isolated trees.

Table 2. Description of land cover classes used in this study.

Class	Description
Montane forest	Closed-canopy evergreen forests of the Eastern Arc Ecoregion [81]
Closed woodland	Areas Dominated by closed tree vegetation; tree plantations other than teak may be included
Open woodland	Sparse tree vegetation, mainly Miombo dry forests (*Brachystegia longifolia*), and to a minor degree plantations in early stages of afforestation
Teak plantation	Commercial teak plantation (*Tectona grandis*); few other species may be present in the understory, but to a negligible degree
Swamp	Shrubby vegetation adapted to waterlogged soils
Grassland	Natural flood grassland dominated by sedges such as *Cyperus distans* [11]
Savanna	All non-flooded open grasslands; usually with isolated trees [11]
Upland agriculture	Maize, tubers, vegetables and other food crops usually grown in mosaics of small patches and in crop rotation
Rice	Lowland rice agricultural fields
Built-up	Man-made artificial surfaces like metals or tarmac
Water	Open water, including streams, ponds, and lakes

The 60 image bands (five multitemporal metrics for each of the six spectral bands and the six spectral indices) were stacked together with the topographic properties of the DEM (elevation, slope, TPI, SV, TRI, TWI) and subjected to a random forest (RF) supervised classification [82]. Yielding high accuracy rates, RF classifier is more and more used in different domains, including wetland monitoring [83,84]. In this study, we used the free and open-source randomForest package [85] in the R statistical software [86]. RF is an ensemble classifier based on decision trees, contributing to a 'forest'. For each tree, a random and independent bootstrapped sample (in bag) from the original input dataset is used to determine the tree's split values, best-reducing entropy among the samples' values, and the result is evaluated with the remaining samples (out of bag). From these, the so-called out of bag error (OOB) is estimated as an internal validation. Among its advantages are the convergence instead of overfitting when using large numbers of trees [82] and the non-parametric nature, which means independence from strong *a priori* assumptions about the statistical characteristics of a class [87]. RF have proven to handle categorical data, imbalanced data, and data with missing values and insignificant features well with similar performances than other classifiers like Support Vector Machines (SVM) [88]. Also, it provides the relative importance of predictive variables by removing a variable for each tree and subtracting the resulting accuracy from the original one. For normalization of that value, the raw variable importance is divided by its standard deviation. High values indicate high importance for the whole RF model [89,90]. The ability to evaluate the model internally with the OOB error can be seen as an advantage, but with caution. Although this error can serve as an approximation, this estimation can differ significantly from an independent accuracy assessment and should in any case be complemented by one, as shown by [84]. As a general advantage of ensemble classifiers, along with the final classification, the classifier provides the option to draw a probability map that consists of the distribution of votes of the single tree classifier components. The vote distribution across classes, for example measured as entropy, can be seen as an estimate of classification uncertainty across the study area and used as additional quality criterion [91]. For the classification reference, we split the data

randomly into 60% for training and 40% for validation. Thus, in a stratified context, small classes were intentionally oversampled, a common practice in the use of imbalanced training data [92]. We found that buffering the reference points resulted in consistently higher classification accuracies and therefore buffered built-up and water by 30 m (in order to retain pure pixels we kept the buffer small) and all other classes by 75 m. All other tests to improve the classification performance (e.g., feature selection, different training/validation data splits) resulted in negligible differences. The number of trees was set to 500; the number of variables tried at each split was 6 for 1974, 24 for 1994 and 32 for 2004 and 2014.

2.5. Change Assessment

We used PCC to quantify the changes of the 40-year study period [27]. Interpretation of the resulting maps is simple and statistics can be calculated based on 'from-to' classes independently from the original data used for the classifications [93]. Subtle land-cover changes can be interpreted as modification of a landscape unit without necessarily changing its classification. Hence, spectral changes may occur due to anthropogenic activity or climate variability that does not translate in a different land use class. Therefore, we also assessed spectral changes in addition to the PCC. Multitemporal metrics represent pseudo-spectral bands rather than spectral measurements. We achieved spectral comparability between the time steps by selecting the most appropriate bands with an all-against-all correlation analysis. We used percentiles of TC brightness, greenness, and wetness at 5% intervals and correlated them between consecutive time steps (e.g., minimum brightness 2004 against minimum brightness 2014, 5th percentile brightness 2004 against minimum brightness 2014 and so forth). The TC components were selected because of their physical interpretability and their comparability across Landsat sensors. Based on the assumption that the highest correlation includes least spurious changes, we calculated Pearson's correlation coefficient and selected those band pairs that showed highest correlation. With only a few exceptions the mean values yielded highest correlation. For each consecutive reference year, we generated a TC component stack from the bands that showed the highest correlation and performed change detection based on the robust change vector analysis (RCVA) [94], a modification of the well-known change vector analysis (CVA) [95]. For example, the 40th percentile brightness 2004, mean greenness 2004, and mean wetness 2004 were assessed against the 35th percentile brightness 2014, mean greenness 2014, and mean wetness 2014. This variant of the well-known change vector analysis provides information about change intensity expressed as magnitude, and the nature of change expressed as direction [94,96–98]. Change direction can be calculated in different ways. Here, we applied coding according to increase or decrease in each index band difference [98]. Using three bands, this results in only eight values (directions), each of them providing a unique combination of increase or decrease in the TC components. We applied the Otsu threshold method [99] on each magnitude image to separate changes from unchanged areas and applied the resulting binary mask on both images, magnitude and direction. A combination of PCC and RCVA change results allowed us to distinguish areas that show no change, areas where only PCC or only RCVA recorded changes and those where both methods detected changes. PCC reveals changes related to the conversion of land use classes to other classes, whereas RCVA is more suited to detect within-class spectral changes. These can be related for example to forest growth or selective logging and other forms of degradation. Sometimes these spectral changes indicate the beginning of land conversion at sub-pixel scale and are therefore important to locate potential future LULC changes.

2.6. Accuracy Assessment and Evaluation of Classification Results

We calculated overall accuracy, user's accuracy, and producer's accuracy, well-established measures of accuracy which are all averaged across space [100], following the suggestions by Olofsson et al. (2014) [101]. Also, authors increasingly explore map quality and spatial uncertainty, which complement regular accuracy measures [91]. Many studies applying RF do not further consider the class probabilities. In contrast, we calculated individual class probabilities within the RF classification to account for the level of classifier-internal uncertainty [84]. As additional measure,

we calculated Shannon's entropy which shows how distinct the class votes for each pixel are. Low entropy indicates only little confusion between classes and a concordant decision whereas high entropy denotes ambiguity. Hence, sources of uncertainty crystallize in low probability levels for the resulting class and high entropy, whereas areas of high probability and low entropy values for the resulting class can be called areas of low internal uncertainty. Here, we additionally calculate the highest probability per pixel from the per-class probabilities to identify areas with high and low classification confidence. In addition, we determined the second highest probability and calculated the difference between highest and second highest probability. This difference shows how dominant a class score is. Low probabilities do not necessarily translate into misclassification, but understanding misclassification can help to interpret mapped LULC changes.

RF final class decision results from the most popular class vote from all trees [82]. The proportions can be translated to probabilities, where a high probability does not necessarily mean that a pixel is correctly classified. However, high values indicate a high probability of a pixel to belong to certain class. A pixel therefore does not need to have probabilities higher than 50% in order to be assigned to a class. Higher ambiguities can be expected from those pixels that are assigned to a class with votes of less than 50% of the trees. We looked on all pixels with less than 50% maximum classification probability, determined the class with second highest classification probability, and calculated for each class the percentages of the second-placed classes. Whereas this cannot be used as a validation measure it reveals dominant confusion and hence similarities in feature space.

3. Results and Discussion

3.1. LULC Classification

Most of the selected classes are of continuous nature making it challenging to distinguish them. For example, floodplain grassland and savanna are both dominated by grass species; rainfed crops and grasses have similar phenology; and open and closed woodland are at the ends of a continuum. However, we achieved consistent classification results with reasonable overall accuracies between 64% and 74% based on validation with independent data (Tables 3–6). Internal classifier performance was good with low OOB errors ranging between 3.28% and 6.67% (see Supplementary Materials). Most classes had high user's and producer's accuracies, in particular the forest classes. Built-up areas are very small in extent compared to the other classes and therefore show low producer's accuracy. Confusion also exists between savanna and grassland, and between upland agriculture and rice crops. Indeed, it is common practice to grow rice as the main crop and other food crops such as maize and vegetables during the small rainy season or in the dry season. With the present approach, we are not able to account for these management practices but rather classify the dominant crop.

Table 3. Error adjusted area estimates of the 1974 classification. Accuracy measures are presented with 95% confidence interval (PA = producer accuracy, UA = user accuracy, OA = overall accuracy).

.	Estimated Area (ha)	PA	UA	OA
Built-up	49,986 ± 38,294	NA ± NA	0 ± 0	
Closed woodland	1,017,708 ± 129,363	0.79 ± 0.08	0.70 ± 0.09	
Upland agriculture	171,522 ± 67,311	0.45 ± 0.18	0.30 ± 0.17	
Grassland	307,336 ± 68,440	0.62 ± 0.11	0.62 ± 0.10	
Montane forest	225,514 ± 59,647	0.91 ± 0.08	0.65 ± 0.14	
Open woodland	1,555,438 ± 172,343	0.60 ± 0.08	0.82 ± 0.06	
Rice	43,454 ± 31,315	0.30 ± 0.30	0.12 ± 0.21	
Savanna	416,565 ± 109,052	0.39 ± 0.13	0.27 ± 0.12	
Swamp	162,247 ± 63,953	0.54 ± 0.19	0.33 ± 0.18	
Water	73,495 ± 40,386	0.83 ± 0.15	0.08 ± 0.16	
				0.63 ± 0.04

Table 4. Error adjusted area estimates of the 1994 classification. Accuracy measures are presented with 95% confidence interval (PA = producer accuracy, UA = user accuracy, OA = overall accuracy).

	Estimated Area (ha)	PA	UA	OA
Built-up	74,992 ± 46,332	0.50 ± 0.27	0.01 ± 0.21	
Closed woodland	1,082,929 ± 122,788	0.86 ± 0.07	0.78 ± 0.08	
Upland agriculture	226,788 ± 79,338	0.46 ± 0.15	0.38 ± 0.13	
Grassland	265,508 ± 51,142	0.65 ± 0.11	0.73 ± 0.09	
Montane forest	144,941 ± 37,997	0.88 ± 0.09	0.82 ± 0.11	
Open woodland	1,541,533 ± 172,020	0.65 ± 0.08	0.84 ± 0.06	
Rice	62,081 ± 30,824	0.40 ± 0.25	0.13 ± 0.33	
Savanna	515,816 ± 123,702	0.46 ± 0.12	0.32 ± 0.12	
Swamp	60,782 ± 34,791	0.52 ± 0.24	0.35 ± 0.21	
Water	48,651 ± 23,308	1.00 ± 0.00	0.18 ± 0.21	
				0.68 ± 0.04

Table 5. Error adjusted area estimates of the 2004 classification. Accuracy measures are presented with 95% confidence interval (PA = producer accuracy, UA = user accuracy, OA = overall accuracy).

	Estimated Area (ha)	PA	UA	OA
Built-up	31,812 ± 21,143	0.78 ± 0.22	0.04 ± 0.14	
Closed woodland	840,967 ± 116,981	0.79 ± 0.09	0.80 ± 0.09	
Upland agriculture	246,539 ± 73,300	0.52 ± 0.15	0.51 ± 0.14	
Grassland	302,467 ± 61,339	0.70 ± 0.11	0.72 ± 0.10	
Montane forest	184,132 ± 45,866	0.93 ± 0.07	0.75 ± 0.13	
Open woodland	1,724,013 ± 162,458	0.75 ± 0.07	0.90 ± 0.05	
Rice	123,057 ± 44,215	0.36 ± 0.18	0.21 ± 0.16	
Savanna	386,400 ± 100,687	0.57 ± 0.13	0.40 ± 0.15	
Swamp	103,921 ± 61,465	0.55 ± 0.24	0.26 ± 0.20	
Teak	62,232 ± 55,031	1.00 ± 0.00	0.09 ± 0.14	
Water	18,479 ± 13,236	1.00 ± 0.00	0.63 ± 0.20	
				0.73 ± 0.04

Table 6. Error adjusted area estimates of the 2014 classification. Accuracy measures are presented with 95% confidence interval (PA = producer accuracy, UA = user accuracy, OA = overall accuracy).

	Estimated Area (ha)	PA	UA	OA
Built-up	48,479 ± 33,320	0.90 ± 0.15	0.07 ± 0.17	
Closed woodland	869,923 ± 109,986	0.83 ± 0.08	0.84 ± 0.08	
Upland agriculture	537,037 ± 117,229	0.54 ± 0.12	0.53 ± 0.12	
Grassland	199,111 ± 36,502	0.70 ± 0.13	0.78 ± 0.11	
Montane forest	168,713 ± 46,562	0.96 ± 0.06	0.72 ± 0.13	
Open woodland	1,459,744 ± 162,273	0.71 ± 0.08	0.86 ± 0.06	
Rice	325,361 ± 67,926	0.65 ± 0.12	0.66 ± 0.11	
Savanna	252,634 ± 90,657	0.56 ± 0.17	0.23 ± 0.20	
Swamp	58,519 ± 35,514	0.78 ± 0.19	0.35 ± 0.23	
Teak	63,456 ± 52,939	1.00 ± 0.00	0.09 ± 0.15	
Water	41,043 ± 33,020	1.00 ± 0.00	0.21 ± 0.19	
				0.71 ± 0.04

Figure 3 shows the classification results of the entire catchment for the 1970s, 1994, 2004, and 2014.

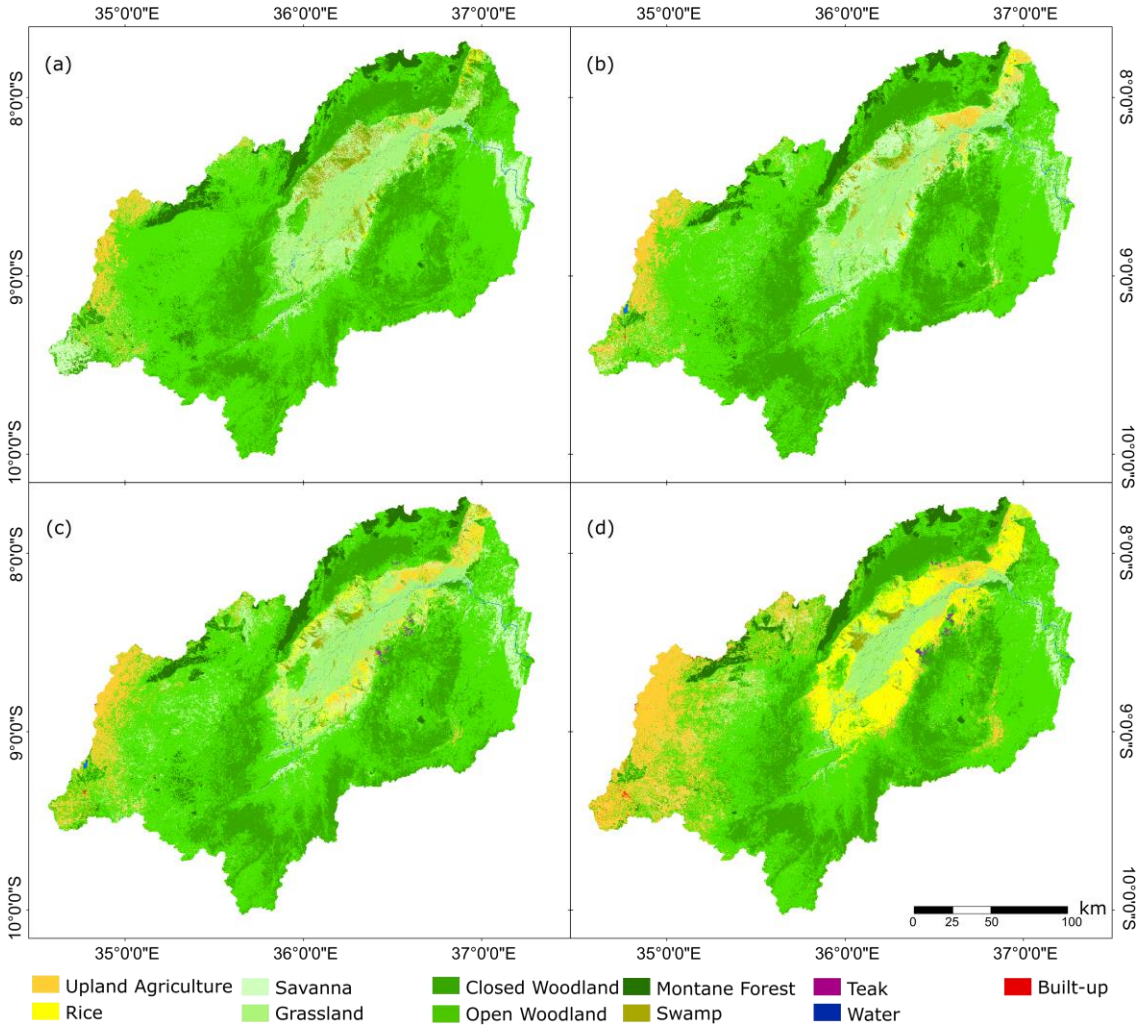

Figure 3. Land use/land cover (LULC) classification results for 1974 (**a**), 1994 (**b**), 2004 (**c**), and 2014 (**d**) for the whole catchment.

Since rice is usually planted within the areas regularly flooded during the rainy season, it can be seen as contrasting to upland agriculture even though typical upland agriculture crops (e.g., maize, vegetables, cassava, sugar cane) are often planted as secondary crops in the same places.

Since the statistical figures of the confusion matrix represent aggregated information over the whole study area, it is useful to assess spatially explicit classifier performance. Figure 4 shows the highest per-pixel probability, the difference between highest and second-highest probability, and entropy. Classification of a pixel is reliable when its highest probability is high, the difference to the second-highest probability is high, and entropy is low (in Figure 4 good performance is indicated by blue colors).

Distinct patterns show across all classifications with higher uncertainty in the floodplain where savanna, grassland, open woodland and upland agriculture are more likely to be confused. This can be explained by higher variability as compared to stable classes like montane forest and teak, by co-occurrence of those classes in small-sized mosaics, crop rotation as well as by spectral similarities. On the one hand, the use of multitemporal metrics over the period of three years leads to robust data to be analyzed. On the other hand, multitemporal metrics reduce the spectral contrast between spectrally related classes, potentially contributing to class confusion. Other studies confirm that temporal aggregation does not necessarily lead to higher classification accuracies compared to well-chosen two-date images [102]. However, in our study selection of appropriate images was not an option due

to persistent cloud cover and due to the size of the study area. To get a better understanding of the per-class RF performance, the reader is referred to the supplementary material that shows the per-pixel classification probability per class.

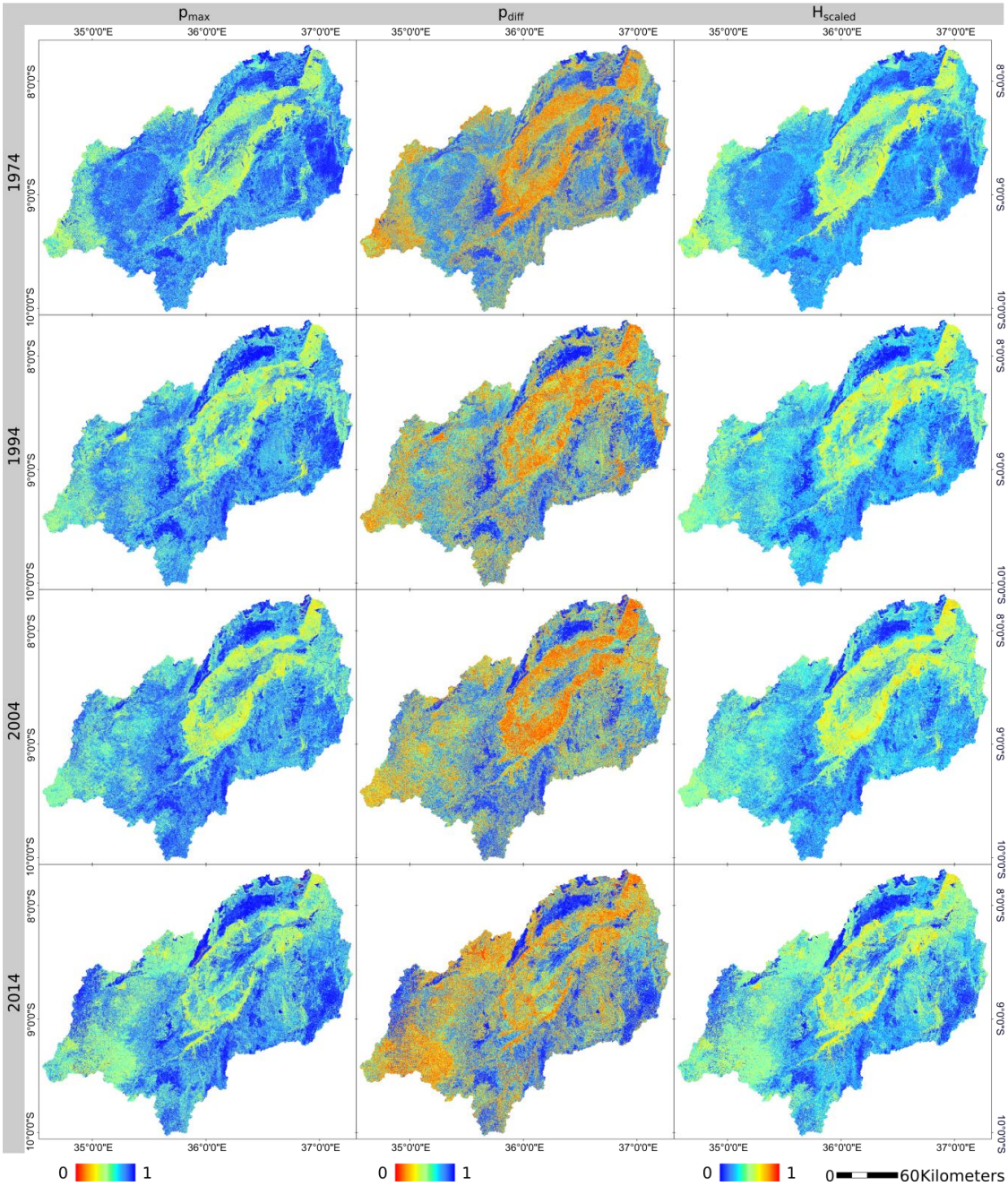

Figure 4. Maximum probability per pixel (P_{max}) achieved by the random forest (RF) classifier for each year (left column). The higher the value, the more reliable the classification. The difference of the highest and the second highest probability per pixel (p_{diff}) are shown in the center column. Higher values indicate less confusion with one or more other classes. The right column shows entropy per pixel scaled between 0 and 1 (H_{scaled}), where 0 indicates unambiguous classification and high values indicate that other classes are to be considered. In all columns red indicates ambiguous results and blue indicates good performance and unambiguous results.

The assessment of the pixels with less than 50% classification probability considered the second-placed class. As a result, it is possible to plot confusion percentages per class (Figure 5). It can be seen that the similarity in feature space is rather stable over time, e.g., the second-placed classes of all montane forest pixels classified with less than 50% probability are open and closed woodland with only a few swamp and water pixels in 1974 and 1994 (Figure 5a,b).

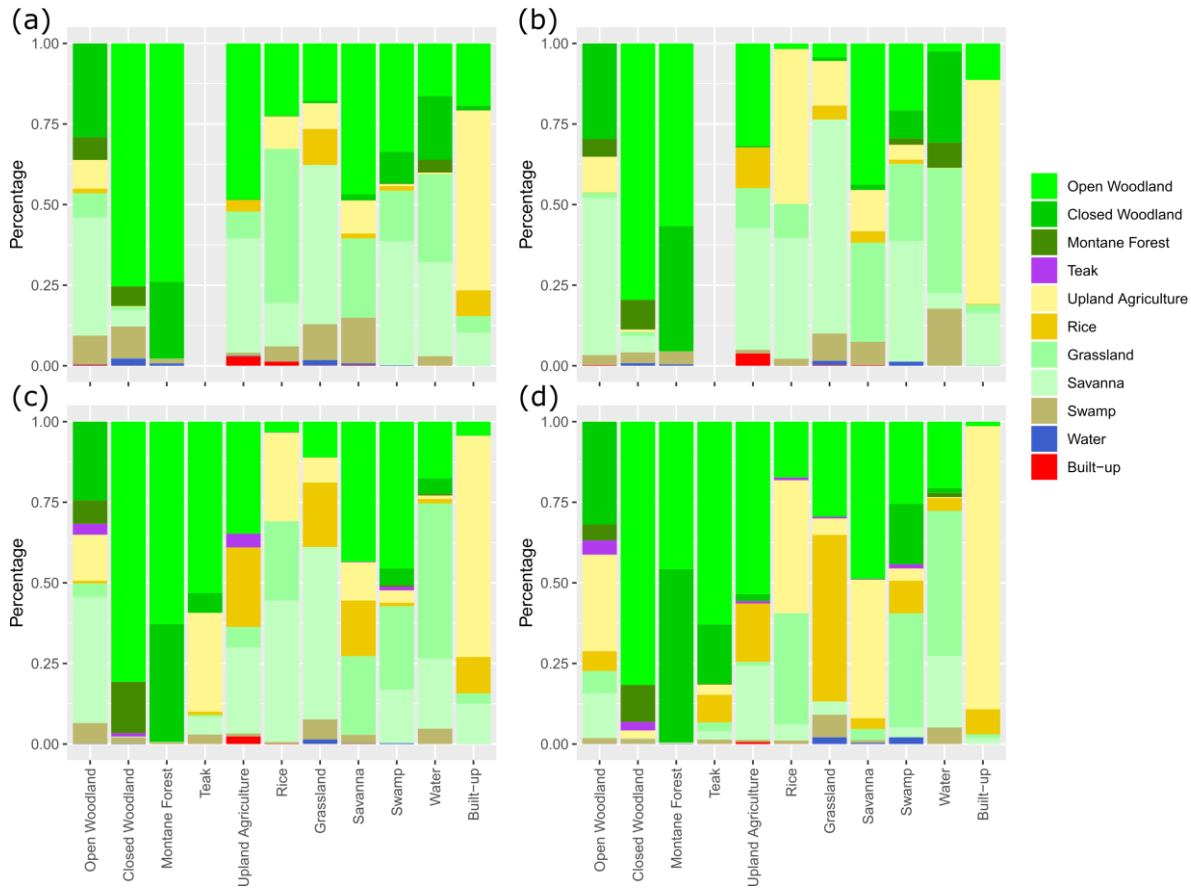

Figure 5. Percentages of classes with second highest classification probability in areas with less than 50% classification probability, (**a**) 1974, (**b**) 1994, (**c**) 2004, (**d**) 2014. Please note: teak was not classified in 1974 and 1994.

This is in line with gradient nature between dense montane forests, closed woodland and open woodland. Hence, open woodland has similarity with montane forest, closed woodland, and savanna. Most likely because there are only scattered trees in the floodplain grassland only little similarity exists with this class. There is however increasing similarity with upland agriculture. Small-scale agricultural fields are often covered by trees and might lead to this kind of confusion. Exploring pixels with less than 50% classification probability focuses on pixels that are likely to be confused with other classes. In turn, if we explore pixels with high probabilities, confusion is likely to include classes that are less well defined. This mainly refers to built-up, which has the largest probability to include mixed pixels. The general pattern of similarity between first and second-ranked classes of pixels with high classification probability (>75%, Figure 6) and those with higher ambiguity (probability <50%, Figure 5) is identical with the exception of higher shares of built-up when the classification probability of the first class is high. The percentage of pixels with classification probabilities lower or higher than 50% is shown in Table 7. It can be seen that more than 80% of all pixels are classified with more than 50% of the votes for a particular class. Some classes are more challenging and show a high percentage of pixels with less than 50% classification probability, e.g., built-up, grassland and rice.

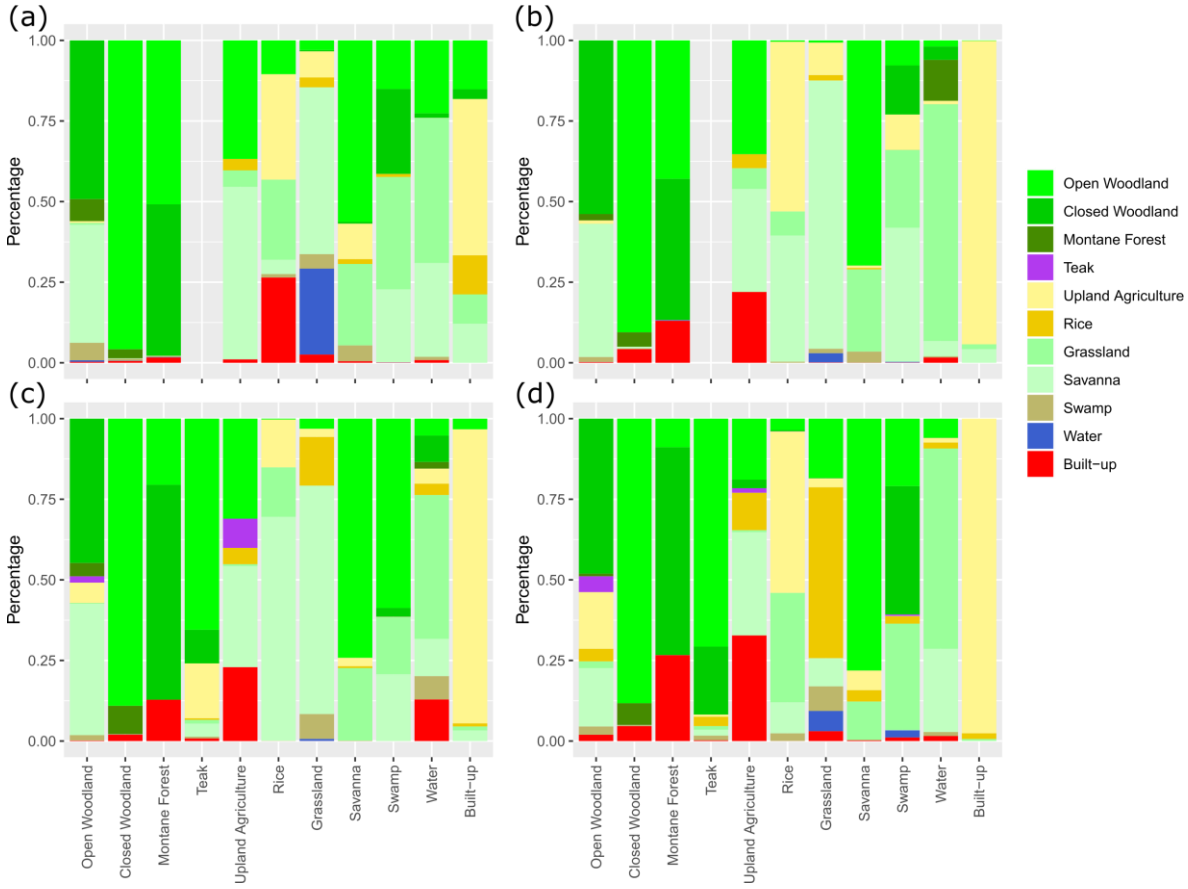

Figure 6. Percentages of classes with second highest classification probability in areas with more than 75% classification probability, (**a**) 1974, (**b**) 1994, (**c**) 2004, (**d**) 2014. Please note: teak was not classified in 1974 and 1994.

Table 7. Percentage of pixels with classification probabilities lower and higher than 50%.

	1974		1994		2004		2014	
	< 50%	> 50%	< 50%	> 50%	< 50%	> 50%	< 50%	> 50%
Open Woodland	9.94	90.06	9.74	90.26	11.36	88.64	17.13	82.87
Closed Woodland	5.71	94.29	5.37	94.63	5.18	94.82	8.10	91.90
Montane Forest	8.61	91.39	11.18	88.82	14.79	85.21	14.30	85.70
Teak	-	-	-	-	54.46	45.54	62.19	37.81
Upland Agriculture	36.53	63.47	34.63	65.37	34.74	65.26	29.58	70.42
Rice	62.04	37.96	77.76	22.24	80.64	19.36	30.92	69.08
Grassland	24.17	75.83	27.69	72.31	30.78	69.22	28.54	71.46
Savanna	46.71	53.29	51.29	48.71	53.46	46.54	48.64	51.36
Swamp	53.06	46.94	55.09	44.91	49.57	50.43	33.60	66.40
Water	35.85	64.15	19.58	80.42	18.38	81.62	24.70	75.30
Built-up	89.56	10.44	69.80	30.20	62.36	37.64	14.28	85.72
Total	14.63	85.37	15.76	84.24	17.78	82.22	19.56	80.44

Figure 7 shows snippets of the classification depicting consistency despite remaining image artifacts.

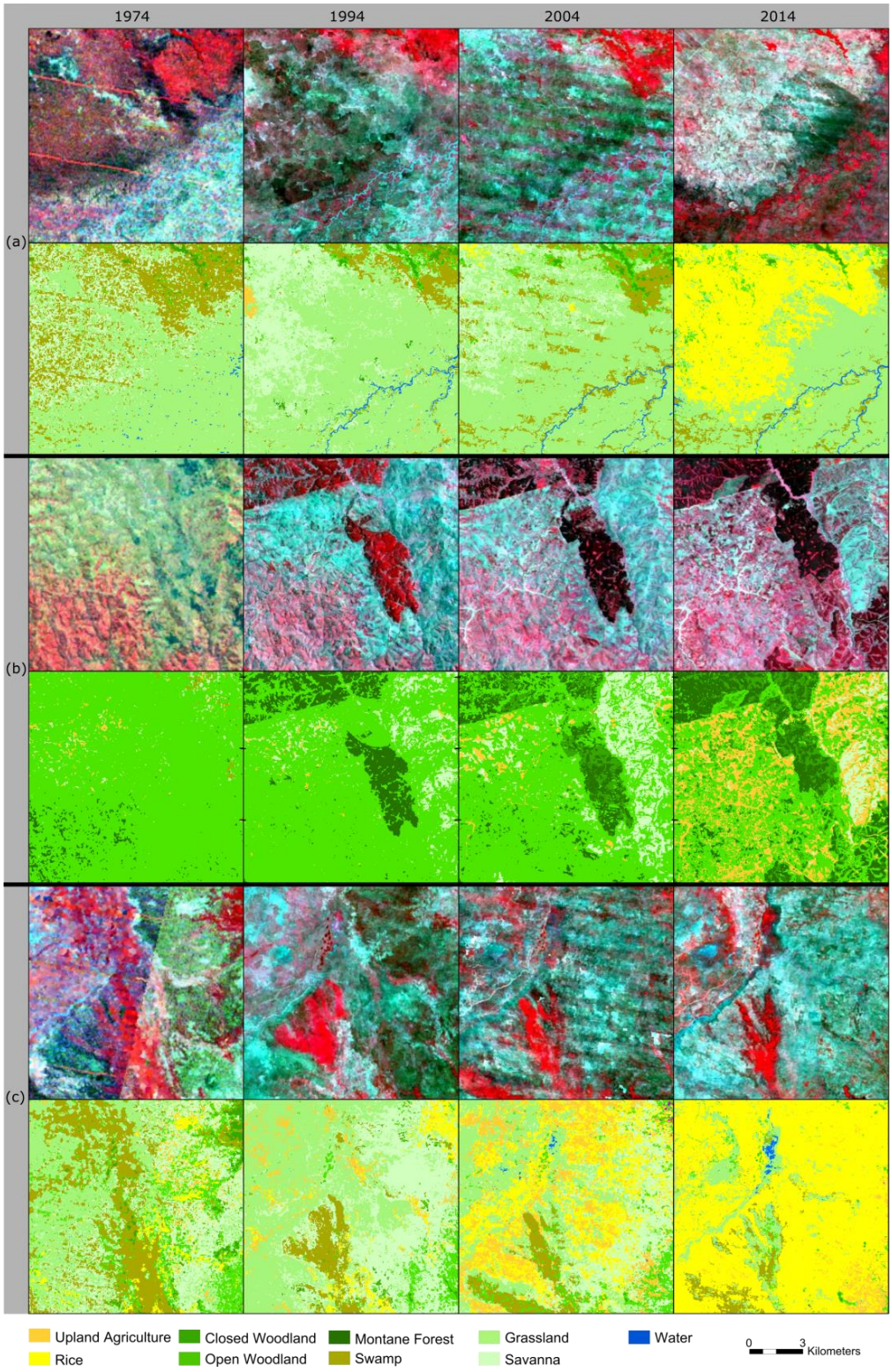

Figure 7. Details of the classification for three different locations (**a**–**c**). Each upper row shows RGB false color composites (mean NIR – mean red – mean green), the lower rows show the respective classification result. (**a**) Conversion of a swamp at the northern margins of the Kilombero floodplain to agricultural land (here: rice). (**b**) Forest plantation in the western part of the catchment. (**c**) Conversion of swamps, floodplain grassland, and savanna to cropland used for rice cultivation (southern part of the floodplain). Even though some artifacts are visible, the RF classifier is capable of producing consistent and useful maps. Only a few isolated pixels are visible.

3.2. LULC Change

We assessed two different types of change: 1. LULC conversion, i.e., replacement of a LULC class by another, and 2. spectral changes. The latter usually apply for LULC conversion but also for modification, i.e., within-class changes that do not necessarily translate in a different classification. LULC conversion is visible in Figure 3 which reveals most pronounced changes within the Kilombero floodplain where natural grasslands, savanna vegetation and swamps were converted to agricultural areas with rice dominating in the flood prone areas. It also becomes obvious that the changes accelerated between 2004 and 2014. Apart from the obvious LULC conversion, spectral changes are evident in huge parts of the study site (Figures 8 and 9).

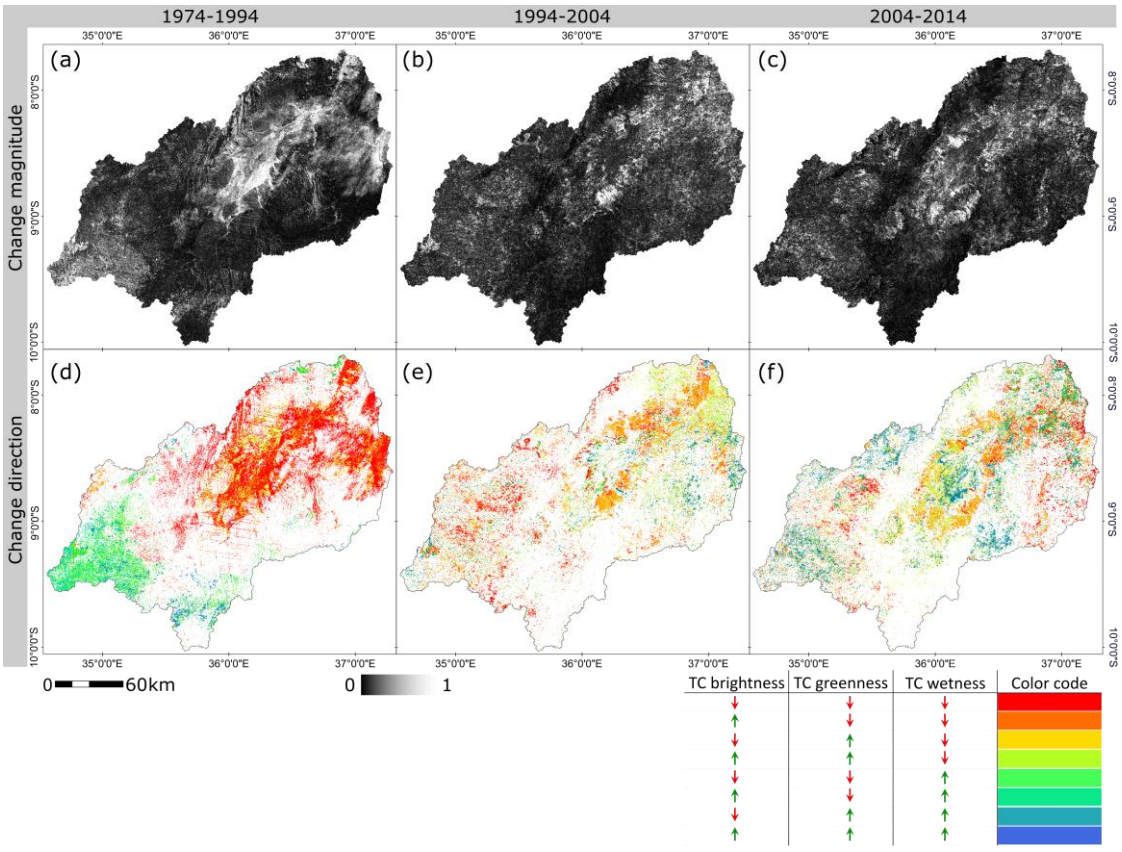

Figure 8. Robust change vector analysis (RCVA)-based spectral change detection results: change magnitude (**a**–**c**), and change direction (**d**–**f**). Change direction is indicated only in places where change magnitude exceeds a threshold (TC = tasseled cap).

High values of RCVA magnitude indicate strong spectral changes whereas values close to zero indicate unchanged areas. The thresholds separating change from no-change were calculated based on the magnitude histograms using the Otsu thresholding method [99]. Figure 8 shows that pronounced spectral changes between 1974 and 1994 appear in the floodplain and the eastern part of the catchment, but also the western part shows some change. These changes might result from undesired atmospheric effects caused by high water vapor concentration within the Kilombero valley, as indicated by the respective change direction. Changes in the western part (blueish-greenish colors in Figure 8d) are characterized by decreasing TC greenness–most likely due to dryer conditions or due to removal of vegetation that might be attributed to agricultural activities and clearing of natural vegetation. This area (Njombe region) is comparably well developed with infrastructure (Figure 1) and well known for maize, Irish potato, tea and flower production. There are, however, only a few areas affected by LULC conversion between 1974 and 1994. The central southern and northern parts of the catchment show

little spectral changes between 1994 and 2004, and between 2004 and 2014 (Figure 8b,c). The areas showing changes are located within the Kilombero floodplain and in the western part of the catchment. The change directions reveal increasing brightness and decreasing greenness and wetness within the Kilombero floodplain indicating replacement of natural vegetation and pronounced periods with land left bare. A comparison of PCC results and RCVA-based change results shows that both do not entirely overlap. If classes are spectrally similar it may happen that their classification changes from one period to the next, e.g., closed woodland is replaced by open woodland. The respective spectral change, however, may lie below the threshold and is therefore not recorded as change. In other places spectral changes may occur without necessarily changing the classification of a pixel. However, areas where PCC and spectral changes overlap are very likely to show distinct alterations of the bio-physical properties. Areas with highest ambiguities (Figure 4) correlate with areas of most pronounced spectral changes (Figure 8a–c).

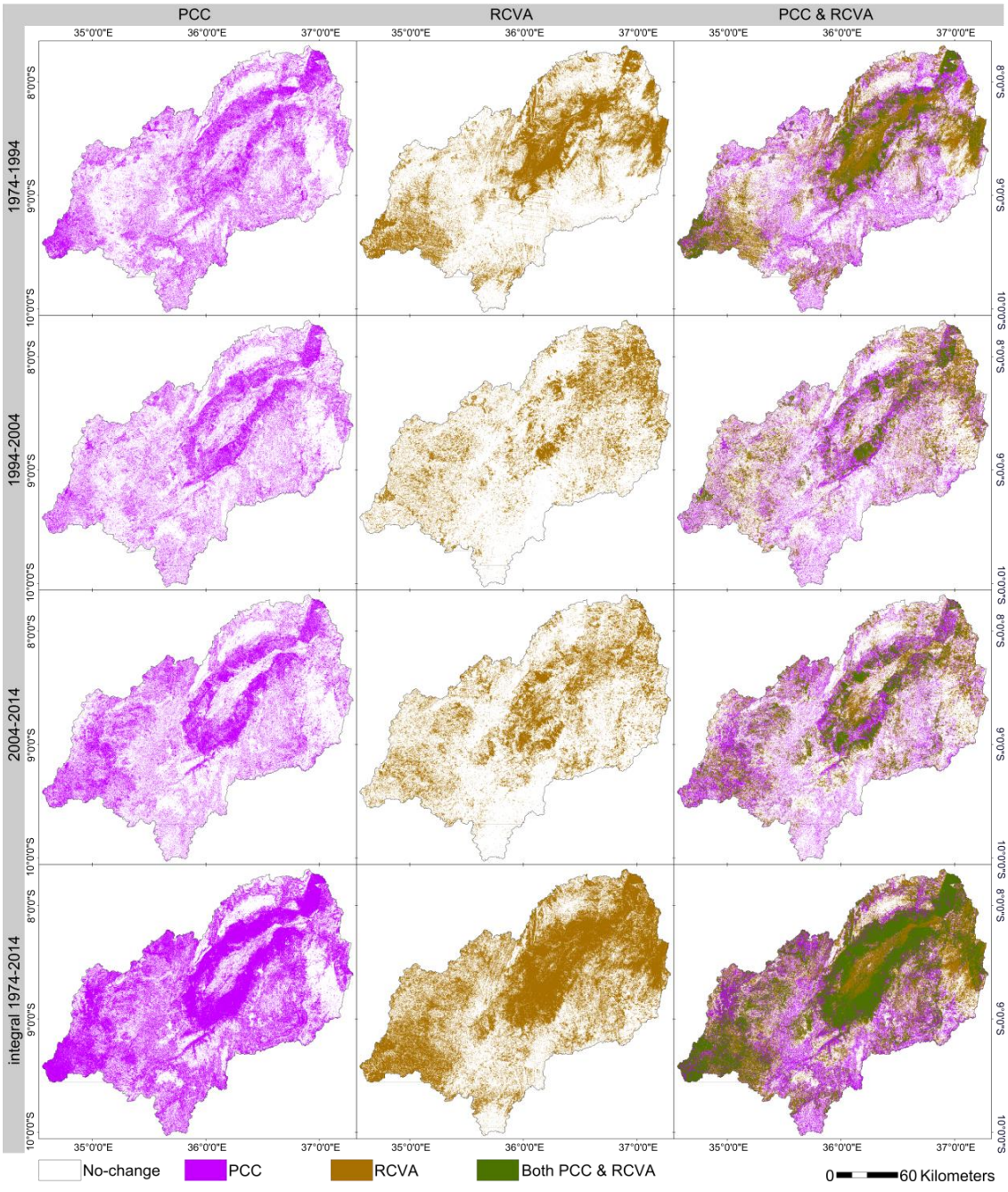

Figure 9. Post-classification comparison (PCC)-based (left) and spectral (center column) changes, and overlay of both (right). The bottom row shows the overlay of all periods (i.e., 1974–2014); the bottom right plot shows the overlay of all periods and both methods. White areas experienced no change, magenta areas denote PCC-based changes, brown areas show RCVA-based spectral changes, and green areas show both PCC and spectral changes.

Maps of the overlaps of the PCC results, the overlaps of the spectral RCVA-based changes, and the overlaps of both of them are shown in Figure 9. There are only a few larger areas that have not changed at all during the observation period (white areas in Figure 8f). They amount to 927,739 ha corresponding to less than one-quarter of the catchment. At the same time, about 1,440,899 ha show both, PCC-based and spectral changes corresponding to about one-third of the catchment area. Those areas are dominant in the Kilombero floodplain and in the west. Fluxes of LULC classes are depicted in the Sankey plots of Figure 10. Looking at the entire catchment area reveals that extension of agricultural areas (upland agriculture and rice cultivation) is the dominant type of change (a). However, a closer look to the Ramsar site shows that rice became the dominant LULC class in this protected area over the past period (b). The Sankey plots also reveal that rice extension is at the expense of savanna and grassland whereas upland agriculture takes place mainly at the expense of open woodland.

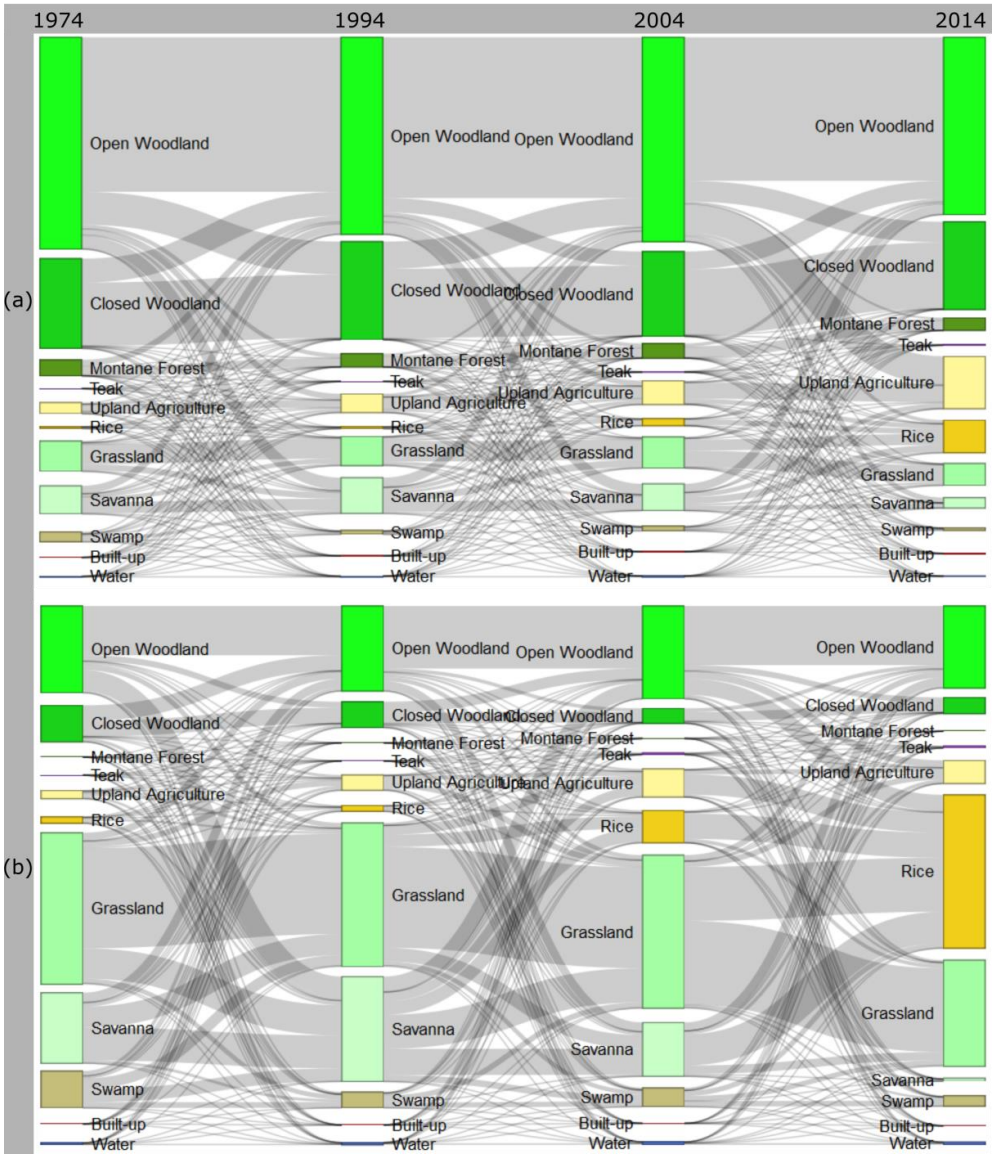

Figure 10. Sankey plots of the LULC changes (**a**) within the whole Kilombero catchment, and (**b**) within the Kilombero Ramsar site.

Land cover conversion in the Kilombero catchment strongly accelerated within the past two decades, resulting in a range of documented effects. LULC changes within the whole catchment have an impact on the hydrological and energy budget of the Kilombero floodplain [12,25]. The feedback loops between LULC change, hydrology and climate are yet to be understood [12,13]. Drivers of change were not addressed in this study but were examined by Msofe et al. (2019) [22] and addressed by Daconto et al. (2018) [103] in the Kilombero valley integrated management plan. According to our findings most intense LULC changes are visible within the Ramsar site, whose extent coincides with the floodplain for the most part. The detected changes are dominated by increased conversion to agriculture, in particular by rice cultivation after 2004. This LULC conversion mostly affected savanna and floodplain grassland, which declined over the past years. Only 1900 km^2 of floodplain grassland remain. This trajectory can be explained by the growing population in-situ as well as through migration, but also reflects governmental strategies [22,40]. While there is a lack of wetland inventories in Africa and hence only limited knowledge about wetland extent and change, a general decline of wetlands is evident [3,5,104], which is in line with our results. A recent LULC change assessment in the Wami river basin in Tanzania revealed similar results to our study with a remarkable decline of grassland and woodland resulting from a conversion to cultivated land [105]. By buying the land, domestic and foreign investors push the local farmers into the wetland and the forests. Increased forest use intensity does not necessarily translate into LULC change between forest classes or in forest loss.

Food production is of high priority in Tanzania, as reflected by Tanzania's *kilimo kwanza* (agriculture first) strategy entailing modernization of agriculture. In particular, this manifests in the implementation of the SAGCOT in the Kilombero catchment. However, the cropland area within the Kilombero floodplain spreads along the margins of the floodplain, leaving only little space for further changes. Crop production increasingly extends inside the flooded areas with the risk of drowning crops. About 7250 km^2 of the catchment's natural vegetation, predominantly grassland and savanna were converted to cropland since the 1970s ($\triangleq$ 18% of the catchment area); most of the changes occurred between 2004 and 2014. Suitable food production areas are exploited almost to their limits. Further LULC conversion can only take place at the expense of natural woodland or within the floodplain. Going further inside the floodplain will only work if the Kilombero floods are regulated, which could have dramatic negative impacts on the ecosystem. For the study period, agricultural expansion into forests is of minor importance. Converting forest to cropland impacts hydrological processes since the forests are the place where runoff and groundwater discharge are generated [12]. In addition, forest loss would directly translate into further habitat loss, biodiversity loss and negative impacts on local livelihoods that depend on their ecosystem services. Hence, further agricultural development must rely on measures to increase productivity, e.g., moderate irrigation, use of fertilizer, leveling, weeding, bunding [106,107]. Such options must be weighed carefully, as also agricultural intensification without areal extension can have detrimental effects on the environment, if not done in a sustainable manner, causing soil compaction, erosion or pollution through input of chemicals [108]. Nevertheless, good agricultural practices can improve yields but are currently not common practice in the Kilombero area [107]. Intensification, however, requires financial capital, access to fertilizer, and capacities. All these measures must be balanced with the guidelines of the different protected areas that cover vast areas of the Kilombero catchment. A management plan was established in late 2018, which outlines various scenarios depending on the funding [103]. It forms a policy framework for future sustainable development in the region. Our LULC maps are integral part of it, and continuous monitoring may support those efforts [20]. LULC often results in extensive loss of ecosystem services [23,109]. Hence, our LULC change assessment may serve to quantifying related ecosystem services.

4. Conclusions

Long-term LULC change assessments with dense time series of satellite imagery are often used to generate a comprehensive understanding of landscape changes and natural resources management. Despite a large historical data record provided by the Landsat program, change analyses carried out in tropical wetlands face limited availability of usable data due to persistent cloud cover triggered by excessive moisture. It is precisely in these environments where LULC change analyses are needed the most, due to the intense expansion of agriculture and urban environments experienced during this century. In this study, we demonstrate an appropriate approach to LULC analysis using multitemporal metrics of Landsat data. We generated decadal gapless composites that reflect seasonal patterns and are comparable between years, achieving reasonable classification accuracies for these dynamic environments. The analysis of per-pixel classification probabilities and derived parameters, as performed here, is well suited to detect spatial patterns of classification reliability and to support the interpretation of the results. Our combined approach of spectral change detection and PCC revealed complementarity, since LULC conversion and subtle within-class changes could be identified. Using least correlated multitemporal metrics of TC components allowed us to minimize spurious changes. Our results also showed that the area of land per capita for agricultural development is becoming increasingly scarce in the Kilombero catchment. Almost half of the Kilombero Ramsar site, a protected area with international importance, was converted from natural to anthropogenic land use, mostly during the 21st century. Located alongside a widely unregulated river system the Kilombero wetland is still a precious ecosystem. Under the current situation of constant economic and population growth and accelerating LULC change over the past decades it is likely that anthropogenic land use expansion will further increase. A regular LULC monitoring may serve as a means to guide decision makers through the process of sustainable land resource management, and to facilitate the implementation and success of such plans.

Supplementary Materials: The following are available online at http://www.mdpi.com/2072-4292/12/7/1057/s1, Figure S1: classification probabilities per pixel and per class, Figure S2: variable importance for the classifications of 1974, 1994, 2004, and 2014, Table S1: Random forest model performance for the 1974 classification, Table S2: Random forest model performance for the 1994 classification, Table S3: Random forest model performance for the 2004 classification, Table S4: Random forest model performance for the 2014 classification, Table S5: From-to-LULC changes between 1974 and 1994, Table S6: From-to-LULC changes between 1994 and 2004, Table S7: From-to-LULC changes between 2004 and 2014.

Author Contributions: Conceptualization, F.T. and S.S.; methodology, F.T. and S.S.; validation, F.T., S.S. and J.M.; formal analysis, F.T. and S.S.; investigation, F.T. and S.S.; data curation, F.K., S.S. and F.T.; writing—original draft preparation, F.T. and S.S.; writing—review and editing, F.T., S.S., J.M. and F.K.; visualization, F.T. All authors have read and agreed to the published version of the manuscript.

Founding: German Federal Ministry of Education and Research: FKZ: 031A250 A-H.

Acknowledgments: This research was conducted within the GlobE - Wetlands in East Africa project, which was funded by the German Federal Ministry of Education and Research (FKZ: 031A250 A-H) with additional funding provided by the German Federal Ministry of Economic Cooperation and Development. We thank Giuseppe Daconto from the Kilombero and Lower Rufiji Wetlands Ecosystem Management Project (KILORWEMP) financed by the European Union and Enabel (Belgian Development Agency) and executed by the Ministry of Natural Resources and Tourism of Government of Tanzania and the Enabel (TAN1102711). He provided aerial photographs and supported this research with his huge local knowledge. We also thank the RapidEye Science Archive (RESA) for providing RapidEye data under proposal 660. J.M. has received funding from the European Union's Horizon 2020 research and innovation program within the Satellite-Based Wetland Observation Service (SWOS) project under Grant Agreement No. 642088. We further thank the anonymous reviewers for their helpful comments.

Conflicts of Interest: The authors declare no conflict of interest. The funders had no role in the design of the study; in the collection, analyses, or interpretation of data; in the writing of the manuscript, or in the decision to publish the results.

References

1. *Land-Use and Land-Cover Change: Local Processes and Global Impacts*; Global Change—The IGBP Series; Lambin, E.F.; Geist, H.J., (Eds.) Springer: Berlin/Heidelberg, Germany, 2006; ISBN 978-3-540-32201-6.

2. Rebelo, L.-M.; McCartney, M.P.; Finlayson, C.M. Wetlands of Sub-Saharan Africa: Distribution and contribution of agriculture to livelihoods. *Wetl. Ecol Manag.* **2010**, *18*, 557–572. [CrossRef]
3. Darrah, S.E.; Shennan-Farpón, Y.; Loh, J.; Davidson, N.C.; Finlayson, C.M.; Gardner, R.C.; Walpole, M.J. Improvements to the Wetland Extent Trends (WET) index as a tool for monitoring natural and human-made wetlands. *Ecol. Indic.* **2019**, *99*, 294–298. [CrossRef]
4. Davidson, N.C.; Fluet-Chouinard, E.; Finlayson, C.M. Global extent and distribution of wetlands: Trends and issues. *Mar. Freshw. Res.* **2018**, *69*, 620. [CrossRef]
5. Ramsar Convention on Wetlands. *Global Wetland Outlook: State of the World's Wetlands and Their Services to People*; Ramsar Convention Secretariat: Gland, Switzerland, 2018.
6. Näschen, K.; Diekkrüger, B.; Evers, M.; Höllermann, B.; Steinbach, S.; Thonfeld, F. The Impact of Land Use/Land Cover Change (LULCC) on Water Resources in a Tropical Catchment in Tanzania under Different Climate Change Scenarios. *Sustainability* **2019**, *11*, 7083. [CrossRef]
7. MacKay, H.; Finlayson, C.M.; Fernández-Prieto, D.; Davidson, N.; Pritchard, D.; Rebelo, L.-M. The role of Earth Observation (EO) technologies in supporting implementation of the Ramsar Convention on Wetlands. *J. Environ. Manag.* **2009**, *90*, 2234–2242. [CrossRef]
8. Rebelo, L.-M.; Finlayson, C.M.; Strauch, A.; Rosenqvist, A.; Perennou, C.; Tøttrup, C.; Hilarides, L.; Paganini, M.; Wielaard, N.; Siegert, F.; et al. *The Use of Earth Observation for Wetland Inventory, Assessment and Monitoring: An Information Source for the Ramsar Convention on Wetlands*; Ramsar Technical Report No. 10; Ramsar Convention Secretariat: Gland, Switzerland, 2018.
9. Darwin, R.; Tsigas, M.; Lewandrowski, J.; Raneses, A. Land use and cover in ecological economics. *Ecol. Econ.* **1996**, *17*, 157–181. [CrossRef]
10. Beck, A.D. The Kilombero valley of south-central Tanganyika. *East Afr. Geogr. Rev.* **1964**, *2*, 37–43.
11. Jätzold, R.; Baum, E. *The Kilombero Valley (Tanzania). Characteristic Features of the Economic Geography of a Semihumid East African Flood Plain and Its Margins*; IFO-Institut für Wirtschaftsforschung München; Weltforum Verlag: München, Germany, 1968.
12. Näschen, K.; Diekkrüger, B.; Leemhuis, C.; Steinbach, S.; Seregina, L.S.; Thonfeld, F.; Van der Linden, R. Hydrological Modeling in Data-Scarce Catchments: The Kilombero Floodplain in Tanzania. *Water* **2018**, *10*, 599. [CrossRef]
13. Senkondo, W.; Munishi, S.E.; Tumbo, M.; Nobert, J.; Lyon, S.W. Comparing Remotely-Sensed Surface Energy Balance Evapotranspiration Estimates in Heterogeneous and Data-Limited Regions: A Case Study of Tanzania's Kilombero Valley. *Remote Sens.* **2019**, *11*, 1289. [CrossRef]
14. Dronova, I.; Gong, P.; Wang, L.; Zhong, L. Mapping dynamic cover types in a large seasonally flooded wetland using extended principal component analysis and object-based classification. *Remote Sens. Environ.* **2015**, *158*, 193–206. [CrossRef]
15. White, L.; Brisco, B.; Dabboor, M.; Schmitt, A.; Pratt, A. A Collection of SAR Methodologies for Monitoring Wetlands. *Remote Sens.* **2015**, *7*, 7615–7645. [CrossRef]
16. Wohlfart, C.; Winkler, K.; Wendleder, A.; Roth, A. TerraSAR-X and Wetlands: A Review. *Remote Sens.* **2018**, *10*, 916. [CrossRef]
17. Johansson, E.L.; Abdi, A.M. Mapping and quantifying perceptions of environmental change in Kilombero Valley, Tanzania. *Ambio* **2020**, *49*, 557–568. [CrossRef] [PubMed]
18. Kato, F. Development of a major rice cultivation area in the Kilombero Valley, Tanzania. *Afr. Study Monogr.* **2007**, *36*, 3–18.
19. Kirimi, F.; Thiong'o, K.; Gabiri, G.; Diekkrüger, B.; Thonfeld, F. Assessing seasonal land cover dynamics in the tropical Kilombero floodplain of East Africa. *J. Appl. Remote Sens.* **2018**, *12*, 1. [CrossRef]
20. Leemhuis, C.; Thonfeld, F.; Näschen, K.; Steinbach, S.; Muro, J.; Strauch, A.; López, A.; Daconto, G.; Games, I.; Diekkrüger, B. Sustainability in the Food-Water-Ecosystem Nexus: The Role of Land Use and Land Cover Change for Water Resources and Ecosystems in the Kilombero Wetland, Tanzania. *Sustainability* **2017**, *9*, 1513. [CrossRef]
21. Meijer, J.; Shames, S.; Giesen, P.; Scherr, S. *Spatial Scenario Modelling to Support Integrated Landscape Management in the Kilombero Valley Landscape in Tanzania. A Case Study on Landscape Strategies to Achieve the Sustainable Development Goals*; PBL Netherlands Environmental Assessment Agency: The Hague, The Netherlands, 2018.
22. Msofe, N.K.; Sheng, L.; Lyimo, J. Land Use Change Trends and Their Driving Forces in the Kilombero Valley Floodplain, Southeastern Tanzania. *Sustainability* **2019**, *11*, 505. [CrossRef]

23. Msofe, N.K.; Sheng, L.; Li, Z.; Lyimo, J. Impact of Land Use/Cover Change on Ecosystem Service Values in the Kilombero Valley Floodplain, Southeastern Tanzania. *Forests* **2020**, *11*, 109. [CrossRef]
24. Munishi, S.; Jewitt, G. Degradation of Kilombero Valley Ramsar wetlands in Tanzania. *Phys. Chem. Earth Parts* **2019**, *112*, 216–227. [CrossRef]
25. Muro, J.; Strauch, A.; Heinemann, S.; Steinbach, S.; Thonfeld, F.; Waske, B.; Diekkrüger, B. Land surface temperature trends as indicator of land use changes in wetlands. *Int. J. Appl. Earth Obs. Geoinf.* **2018**, *70*, 62–71. [CrossRef]
26. Seki, H.A.; Shirima, D.D.; Mustaphi, C.J.C.; Marchant, R.; Munishi, P.K.T. The impact of land use and land cover change on biodiversity within and adjacent to Kibasira Swamp in Kilombero Valley, Tanzania. *Afr. J. Ecol.* **2018**, *56*, 518–527. [CrossRef]
27. Hecheltjen, A.; Thonfeld, F.; Menz, G. Recent Advances in Remote Sensing Change Detection—A Review. In *Land Use and Land Cover Mapping in Europe*; Manakos, I., Braun, M., Eds.; Springer: Dordrecht, The Netherlands, 2014; Volume 18, pp. 145–178. ISBN 978-94-007-7968-6.
28. Midekisa, A.; Holl, F.; Savory, D.J.; Andrade-Pacheco, R.; Gething, P.W.; Bennett, A.; Sturrock, H.J.W. Mapping land cover change over continental Africa using Landsat and Google Earth Engine cloud computing. *PLoS ONE* **2017**, *12*, e0184926. [CrossRef] [PubMed]
29. Colwell, J.E.; Weber, F.P. Forest change detection. In Proceedings of the International Symposium on Remote Sensing of Environment, Ann Arbor, MI, USA, 11–15 May 1981; Volume 15, pp. 839–852.
30. Xian, G.; Homer, C.; Fry, J. Updating the 2001 National Land Cover Database land cover classification to 2006 by using Landsat imagery change detection methods. *Remote Sens. Environ.* **2009**, *113*, 1133–1147. [CrossRef]
31. Leemhuis, C.; Amler, E.; Diekkrüger, B.; Gabiri, G.; Näschen, K. East African wetland-catchment data base for sustainable wetland management. *Proc. Int. Assoc. Hydrol. Sci.* **2016**, *374*, 123–128. [CrossRef]
32. Kottek, M.; Grieser, J.; Beck, C.; Rudolf, B.; Rubel, F. World Map of the Köppen-Geiger climate classification updated. *Meteorol. Z.* **2006**, *15*, 259–263. [CrossRef]
33. Peel, M.C.; Finlayson, B.L.; McMahon, T.A. Updated world map of the Köppen-Geiger climate classification. *Hydrol. Earth Syst. Sci.* **2007**, *11*, 1633–1644. [CrossRef]
34. Lillesø, J.-P.B.; van Breugel, P.; Kindt, R.; Mbago, F.; Moshi, H.N.; Ndangalasi, H.J.; Uronu, L.O.N.; Jamnadass, R.; Graudal, L. *Potential Natural Vegetation of Eastern Africa (Ethiopia, Kenya, Malawi, Rwanda, Tanzania, Uganda and Zambia). Volume 10. Atlas and Tree Species Composition for Tanzania*; Department of Geoscience and Natural Resource Management, University of Copenhagen: Copenhagen, Denmark, 2014; ISBN 978-87-7903-622-2.
35. Koutsouris, A.J.; Chen, D.; Lyon, S.W. Comparing global precipitation data sets in eastern Africa: A case study of Kilombero Valley, Tanzania: Comparing global precipitation data sets in Tanzania, East Africa. *Int. J. Climatol.* **2016**, *36*, 2000–2014. [CrossRef]
36. Ntongani, W.A.; Andrew, S.M. Bird species composition and diversity in habitats with different disturbance histories at Kilombero Wetland, Tanzania. *OJE* **2013**, *3*, 482–488. [CrossRef]
37. Lyon, S.W.; Koutsouris, A.; Scheibler, F.; Jarsjö, J.; Mbanguka, R.; Tumbo, M.; Robert, K.K.; Sharma, A.N.; van der Velde, Y. Interpreting characteristic drainage timescale variability across Kilombero Valley, Tanzania. *Hydrol. Process.* **2015**, *29*, 1912–1924. [CrossRef]
38. RBWO the Rufiji Basin Water Office (RBWO) Discharge Database. Available online: http://www.riversnetwork.org/rbo/index.php/river-blogs/central-africa/item/2055-the-rufiji-basin-water-office-rbwo (accessed on 9 July 2017).
39. Siima, S.B.; Munishi, P.K.T.; Ngaga, Y.M.; Navrud, S. Estimating direct use value of Kilombero Ramsar Site based on market price method. *Tanzan. J. For. Nat. Conserv.* **2012**, *81*, 133–146.
40. Nindi, S.J.; Maliti, H.; Bakari, S.; Kija, H.; Machoke, M. Conflicts over Land and Water Resources in the Kilombero Valley Floodplain, Tanzania. *Afr. Study Monogr.* **2014**, *50*, 173–190.
41. Koskinen, J.; Leinonen, U.; Vollrath, A.; Ortmann, A.; Lindquist, E.; d'Annunzio, R.; Pekkarinen, A.; Käyhkö, N. Participatory mapping of forest plantations with Open Foris and Google Earth Engine. *ISPRS J. Photogramm. Remote Sens.* **2019**, *148*, 63–74. [CrossRef]
42. Vogelmann, J.E.; Gallant, A.L.; Shi, H.; Zhu, Z. Perspectives on monitoring gradual change across the continuity of Landsat sensors using time-series data. *Remote Sens. Environ.* **2016**, *185*, 258–270. [CrossRef]

43. Zhu, Z.; Wang, S.; Woodcock, C.E. Improvement and expansion of the Fmask algorithm: Cloud, cloud shadow, and snow detection for Landsats 4–8, and Sentinel 2 images. *Remote Sens. Environ.* **2015**, *159*, 269–277. [CrossRef]
44. Zhu, Z.; Woodcock, C.E. Object-based cloud and cloud shadow detection in Landsat imagery. *Remote Sens. Environ.* **2012**, *118*, 83–94. [CrossRef]
45. Zha, Y.; Gao, J.; Ni, S. Use of normalized difference built-up index in automatically mapping urban areas from TM imagery. *Int. J. Remote Sens.* **2003**, *24*, 583–594. [CrossRef]
46. Tucker, C.J. Red and photographic infrared linear combinations for monitoring vegetation. *Remote Sens. Environ.* **1979**, *8*, 127–150. [CrossRef]
47. McFeeters, S.K. The use of the Normalized Difference Water Index (NDWI) in the delineation of open water features. *Int. J. Remote Sens.* **1996**, *17*, 1425–1432. [CrossRef]
48. Crist, E.P.; Cicone, R.C. A Physically-Based Transformation of Thematic Mapper Data—The TM Tasseled Cap. *IEEE Trans. Geosci. Remote Sens.* **1984**, *GE-22*, 256–263. [CrossRef]
49. Kauth, R.; Thomas, G. *The Tasselled Cap—A Graphic Description of the Spectral-Temporal Development of Agricultural Crops as Seen by LANDSAT*; Purdue: West Lafayette, IN, USA, 1976.
50. Crist, E.P. A TM Tasseled Cap equivalent transformation for reflectance factor data. *Remote Sens. Environ.* **1985**, *17*, 301–306. [CrossRef]
51. Cazals, C.; Rapinel, S.; Frison, P.-L.; Bonis, A.; Mercier, G.; Mallet, C.; Corgne, S.; Rudant, J.-P. Mapping and Characterization of Hydrological Dynamics in a Coastal Marsh Using High Temporal Resolution Sentinel-1A Images. *Remote Sens.* **2016**, *8*, 570. [CrossRef]
52. Davranche, A.; Poulin, B.; Lefebvre, G. Mapping flooding regimes in Camargue wetlands using seasonal multispectral data. *Remote Sens. Environ.* **2013**, *138*, 165–171. [CrossRef]
53. Schlaffer, S.; Chini, M.; Dettmering, D.; Wagner, W. Mapping Wetlands in Zambia Using Seasonal Backscatter Signatures Derived from ENVISAT ASAR Time Series. *Remote Sens.* **2016**, *8*, 402. [CrossRef]
54. Flood, N. Seasonal Composite Landsat TM/ETM + Images Using the Medoid (a Multi-Dimensional Median). *Remote Sens.* **2013**, *5*, 6481–6500. [CrossRef]
55. Flood, N.; Danaher, T.; Gill, T.; Gillingham, S. An Operational Scheme for Deriving Standardised Surface Reflectance from Landsat TM/ETM+ and SPOT HRG Imagery for Eastern Australia. *Remote Sens.* **2013**, *5*, 83–109. [CrossRef]
56. Frantz, D. FORCE—Landsat + Sentinel-2 Analysis Ready Data and Beyond. *Remote Sens.* **2019**, *11*, 1124. [CrossRef]
57. Frantz, D.; Röder, A.; Stellmes, M.; Hill, J. Phenology-adaptive pixel-based compositing using optical earth observation imagery. *Remote Sens. Environ.* **2017**, *190*, 331–347. [CrossRef]
58. Frantz, D.; Stellmes, M.; Röder, A.; Udelhoven, T.; Mader, S.; Hill, J. Improving the Spatial Resolution of Land Surface Phenology by Fusing Medium- and Coarse-Resolution Inputs. *IEEE Trans. Geosci. Remote Sens.* **2016**, *54*, 4153–4164. [CrossRef]
59. Griffiths, P.; van der Linden, S.; Kuemmerle, T.; Hostert, P. A Pixel-Based Landsat Compositing Algorithm for Large Area Land Cover Mapping. *IEEE J. Sel. Top. Appl. Earth Obs. Remote Sens.* **2013**, *6*, 2088–2101. [CrossRef]
60. Nelson, K.J.; Steinwand, D. A Landsat Data Tiling and Compositing Approach Optimized for Change Detection in the Conterminous United States. *Photogramm. Eng. Remote Sens.* **2015**, *81*, 573–586. [CrossRef]
61. Vuolo, F.; Ng, W.-T.; Atzberger, C. Smoothing and gap-filling of high resolution multi-spectral time series: Example of Landsat data. *Int. J. Appl. Earth Obs. Geoinf.* **2017**, *57*, 202–213. [CrossRef]
62. White, J.C.; Wulder, M.A.; Hobart, G.W.; Luther, J.E.; Hermosilla, T.; Griffiths, P.; Coops, N.C.; Hall, R.J.; Hostert, P.; Dyk, A.; et al. Pixel-Based Image Compositing for Large-Area Dense Time Series Applications and Science. *Can. J. Remote Sens.* **2014**, *40*, 192–212. [CrossRef]
63. Azzari, G.; Lobell, D.B. Landsat-based classification in the cloud: An opportunity for a paradigm shift in land cover monitoring. *Remote Sens. Environ.* **2017**, *202*, 64–74. [CrossRef]
64. Esch, T.; Metz, A.; Marconcini, M.; Keil, M. Combined use of multi-seasonal high and medium resolution satellite imagery for parcel-related mapping of cropland and grassland. *Int. J. Appl. Earth Obs. Geoinf.* **2014**, *28*, 230–237. [CrossRef]
65. Hansen, M.C.; Egorov, A.; Potapov, P.V.; Stehman, S.V.; Tyukavina, A.; Turubanova, S.A.; Roy, D.P.; Goetz, S.J.; Loveland, T.R.; Ju, J.; et al. Monitoring conterminous United States (CONUS) land cover change with Web-Enabled Landsat Data (WELD). *Remote Sens. Environ.* **2014**, *140*, 466–484. [CrossRef]

66. Mack, B.; Leinenkugel, P.; Kuenzer, C.; Dech, S. A semi-automated approach for the generation of a new land use and land cover product for Germany based on Landsat time-series and Lucas in-situ data. *Remote Sens. Lett.* **2017**, *8*, 244–253. [CrossRef]
67. Müller, H.; Rufin, P.; Griffiths, P.; Barros Siqueira, A.J.; Hostert, P. Mining dense Landsat time series for separating cropland and pasture in a heterogeneous Brazilian savanna landscape. *Remote Sens. Environ.* **2015**, *156*, 490–499. [CrossRef]
68. Rufin, P.; Müller, H.; Pflugmacher, D.; Hostert, P. Land use intensity trajectories on Amazonian pastures derived from Landsat time series. *Int. J. Appl. Earth Obs. Geoinf.* **2015**, *41*, 1–10. [CrossRef]
69. Canty, M.J.; Nielsen, A.A. Automatic radiometric normalization of multitemporal satellite imagery with the iteratively re-weighted MAD transformation. *Remote Sens. Environ.* **2008**, *112*, 1025–1036. [CrossRef]
70. Nielsen, A.A. The Regularized Iteratively Reweighted MAD Method for Change Detection in Multi- and Hyperspectral Data. *IEEE Trans. Image Process.* **2007**, *16*, 463–478. [CrossRef]
71. Farr, T.G.; Kobrick, M. Shuttle radar topography mission produces a wealth of data. *Eos Trans. AGU* **2000**, *81*, 583–585. [CrossRef]
72. Santillan, J.R.; Makinano-Santillan, M. Vertical accuracy assessment of 30-m resolution ALOS, ASTER, and SRTM global DEMs overnortheastern Mindanao, Philippines. *ISPRS Int. Arch. Photogramm. Remote Sens. Spat. Inf. Sci.* **2016**, *XLI-B4*, 149–156. [CrossRef]
73. Dinesen, L.; Lehmberg, T.; Rahner, M.C.; Fjeldså, J. Conservation priorities for the forests of the Udzungwa Mountains, Tanzania, based on primates, duikers and birds. *Biol. Conserv.* **2001**, *99*, 223–236. [CrossRef]
74. Riley, S.J.; DeGloria, S.D.; Elliot, R. A terrain ruggedness index that quantifies topographic heterogeneity. *Intermt. Journcal Sci.* **1999**, *5*, 23–27.
75. Ruszkiczay-Rüdiger, Z.; Fodor, L.; Horváth, E.; Telbisz, T. Discrimination of fluvial, eolian and neotectonic features in a low hilly landscape: A DEM-based morphotectonic analysis in the Central Pannonian Basin, Hungary. *Geomorphology* **2009**, *104*, 203–217. [CrossRef]
76. Gallant, J.C.; Wilson, J.P. Primary topographic attributes. In *Terrain Analysis: Principles and Applications*; Wilson, J.P., Gallant, J.C., Eds.; John Wiley & Sons: New York, NY, USA, 2000; pp. 51–85.
77. Jenness, J. *Topographic Position Index (tpi _jen.avx) extension for ArcView 3.x*; Version 1.2; Jenness Enterprises: Flagstaff, AZ, USA, 2006.
78. Beven, K.J.; Kirkby, M.J. A physically based, variable contributing area model of basin hydrology/Un modèle à base physique de zone d'appel variable de l'hydrologie du bassin versant. *Hydrol. Sci. Bull.* **1979**, *24*, 43–69. [CrossRef]
79. Evans, J.S.; Oakleaf, J.; Cushman, S.A.; Theobald, D. An ArcGIS Toolbox for Surface Gradient and Geomorphometric Modeling. version 2.0-0. 2014. Available online: http://evansmurphy.wix.com/evansspatial (accessed on 28 January 2020).
80. Planet Rapid Eye Imagery Product Specifications. Version 6.1. 2016. Available online: https://www.planet.com/products/satellite-imagery/files/160625-RapidEye%20Image-Product-Specifications.pdf (accessed on 28 January 2020).
81. Platts, P.J.; Burgess, N.D.; Gereau, R.E.; Lovett, J.C.; Marshall, A.R.; McCLEAN, C.J.; Pellikka, P.K.E.; Swetnam, R.D.; Marchant, R. Delimiting tropical mountain ecoregions for conservation. *Environ. Conserv.* **2011**, *38*, 312–324. [CrossRef]
82. Breiman, L. Random Forests. *Mach. Learn.* **2001**, *45*, 5–32. [CrossRef]
83. Corcoran, J.; Knight, J.; Pelletier, K.; Rampi, L.; Wang, Y. The Effects of Point or Polygon Based Training Data on RandomForest Classification Accuracy of Wetlands. *Remote Sens.* **2015**, *7*, 4002–4025. [CrossRef]
84. Millard, K.; Richardson, M. On the Importance of Training Data Sample Selection in Random Forest Image Classification: A Case Study in Peatland Ecosystem Mapping. *Remote Sens.* **2015**, *7*, 8489–8515. [CrossRef]
85. Liaw, A.; Wiener, M. Classification and Regression by randomForest. *R News* **2002**, *2*, 18–22.
86. R Core Team. *R: A Language and Environment for Statistical Computing*; R Foundation for Statistical Computing: Vienna, Austria, 2019.
87. Canty, M.J. *Image Analysis, Classification and Change Detection in Remote Sensing: With Algorithms for Python*, 4th ed.; CRC Press, Taylor & Francis Group: Boca Raton, FL, USA, 2019.
88. Pelletier, C.; Valero, S.; Inglada, J.; Champion, N.; Dedieu, G. Assessing the robustness of Random Forests to map land cover with high resolution satellite image time series over large areas. *Remote Sens. Environ.* **2016**, *187*, 156–168. [CrossRef]

89. Pal, M. Random forest classifier for remote sensing classification. *Int. J. Remote Sens.* **2005**, *26*, 217–222. [CrossRef]
90. Waske, B.; van der Linden, S.; Oldenburg, C.; Jakimow, B.; Rabe, A.; Hostert, P. imageRF—A user-oriented implementation for remote sensing image analysis with Random Forests. *Environ. Model. Softw.* **2012**, *35*, 192–193. [CrossRef]
91. Horning, N.; Leutner, B.; Wegmann, M. Land cover or image classification approaches. In *Remote Sensing and GIS for Ecologists. Using Open Source Software*; Wegmann, M., Leutner, B., Eds.; Pelagic Publishing: Exeter, UK, 2016.
92. Chen, C.; Liaw, A.; Breiman, L. *Using Random Forest to Learn Imbalanced Data*; University of Berkeley: Berkeley, CA, USA, 2004.
93. Singh, A. Review Article Digital change detection techniques using remotely-sensed data. *Int. J. Remote Sens.* **1989**, *10*, 989–1003. [CrossRef]
94. Thonfeld, F.; Feilhauer, H.; Braun, M.; Menz, G. Robust Change Vector Analysis (RCVA) for multi-sensor very high resolution optical satellite data. *Int. J. Appl. Earth Obs. Geoinf.* **2016**, *50*, 131–140. [CrossRef]
95. Malila, W.A. Change vector analysis: An approach for detecting forest changes with Landsat. In Proceedings of the LARS Symposia, West Lafayette, IN, USA, 3–6 June 1980; Volume 385, pp. 326–335.
96. Bovolo, F.; Marchesi, S.; Bruzzone, L. A nearly lossless 2d representation and characterization of change information in multispectral images. In Proceedings of the 2010 IEEE International Geoscience and Remote Sensing Symposium, Honolulu, HI, USA, 25–30 July 2010; pp. 3074–3077.
97. Bovolo, F.; Bruzzone, L. A Theoretical Framework for Unsupervised Change Detection Based on Change Vector Analysis in the Polar Domain. *IEEE Trans. Geosci. Remote Sens.* **2007**, *45*, 218–236. [CrossRef]
98. Michalek, J.L.; Wagner, T.W.; Luczkovich, J.J.; Stoffle, R.W. Multispectral change vector analysis for monitoring coastal marine environments. *Photogramm. Eng. Remote Sens.* **1993**, 381–384.
99. Otsu, N. A Threshold Selection Method from Gray-Level Histograms. *IEEE Trans. Syst. Man Cybern.* **1979**, *9*, 62–66. [CrossRef]
100. Foody, G.M. Status of land cover classification accuracy assessment. *Remote Sens. Environ.* **2002**, *80*, 185–201. [CrossRef]
101. Olofsson, P.; Foody, G.M.; Herold, M.; Stehman, S.V.; Woodcock, C.E.; Wulder, M.A. Good practices for estimating area and assessing accuracy of land change. *Remote Sens. Environ.* **2014**, *148*, 42–57. [CrossRef]
102. Carrasco, L.; O'Neil, A.W.; Morton, R.D.; Rowland, C.S. Evaluating Combinations of Temporally Aggregated Sentinel-1, Sentinel-2 and Landsat 8 for Land Cover Mapping with Google Earth Engine. *Remote Sens.* **2019**, *11*, 288. [CrossRef]
103. Daconto, G.; Games, I.; Lukumbuzya, K.; Raijmakers, F. Integrated Management Plan for the Kilombero Valley Ramsar Site—Foundation Report. Available online: https://kilomberovalley.files.wordpress.com/2019/02/kvrs-imp_foundation-2018-09.pdf (accessed on 15 January 2020).
104. Davidson, N.C. How much wetland has the world lost? Long-term and recent trends in global wetland area. *Mar. Freshw. Res.* **2014**, *65*, 934. [CrossRef]
105. Twisa, S.; Buchroithner, M.F. Land-Use and Land-Cover (LULC) Change Detection in Wami River Basin, Tanzania. *Land* **2019**, *8*, 136. [CrossRef]
106. Alavaisha, E.; Manzoni, S.; Lindborg, R. Different agricultural practices affect soil carbon, nitrogen and phosphorous in Kilombero-Tanzania. *J. Environ. Manag.* **2019**, *234*, 159–166. [CrossRef] [PubMed]
107. Kwesiga, J.; Grotelüschen, K.; Neuhoff, D.; Senthilkumar, K.; Döring, T.F.; Becker, M. Site and Management Effects on Grain Yield and Yield Variability of Rainfed Lowland Rice in the Kilombero Floodplain of Tanzania. *Agronomy* **2019**, *9*, 632. [CrossRef]
108. Kopittke, P.M.; Menzies, N.W.; Wang, P.; McKenna, B.A.; Lombi, E. Soil and the intensification of agriculture for global food security. *Environ. Int.* **2019**, *132*, 105078. [CrossRef]
109. Sharma, R.; Rimal, B.; Baral, H.; Nehren, U.; Paudyal, K.; Sharma, S.; Rijal, S.; Ranpal, S.; Acharya, R.P.; Alenazy, A.A.; et al. Impact of Land Cover Change on Ecosystem Services in a Tropical Forested Landscape. *Resources* **2019**, *8*, 18. [CrossRef]